5-2018

Examination of Shape Variation of the Calcaneus, Navicular, and Talus in Homo sapiens, Gorilla gorilla, and Pan troglodytes

Nicole Lynn Robinson
University of Arkansas, Fayetteville

Examination of Shape Variation of the Calcaneus, Navicular, and Talus in *Homo sapiens*, *Gorilla gorilla,* and *Pan troglodytes*

A thesis submitted in partial fulfillment
of the requirements for the degree of
Master of Arts in Anthropology

by

Nicole Robinson
Indiana University of Pennsylvania
Bachelor of Science in Natural Science, 2016

May 2018
University of Arkansas

This thesis is approved for recommendation to the Graduate Council.

_____
J. Michael Plavcan, Ph.D.
Committee Chair

_____
Claire E. Terhune, Ph.D.
Committee Member

_____
Lucas K. Delezene, Ph.D.
Committee Member

Abstract

Analyses of morphological integration among primates commonly focus on relationships between the face, braincase and base of the skull, as well as the upper and lower dentition, and the within portions of the post-cranial skeleton. Despite the prominence of these studies, the associations between the bones of the foot and their articular surfaces have largely been ignored among primates, even though the foot demonstrates high degrees of variation and modification. This variation offers an ideal opportunity to study the relationship between morphology and locomotion. Because the talus, calcaneus and navicular act together to stabilize the foot in locomotion and form a direct interface with the substrate, they comprise a complex structural unit, and the matching articular surfaces should be tightly integrated. However, preliminary results suggest there is no difference in the magnitude or pattern of integration within and between bones. While there is no systematic difference in the magnitude of correlations distinguishing articular surfaces from non-articular parts of the bones, the pattern of covariation is itself correlated across species for each bone, with correlations among measurements of articular surfaces consistently positive. This suggests at the least that there are shared patterns of integration across species.

Table of Contents

Chapter 1 Literature Review

Introduction

Morphological integration, a term first coined by Olson and Miller (1958), refers to the phenomenon that an organism's individual characters or traits are interdependent and result in the formation of functionally- and developmentally-related units (Cheverud, 1982; Zelditch, 1987). More simply, studies of morphological integration allow us to examine patterns of covariation of features that constitute units/complexes. There are three principal mechanisms by which morphological integration can occur: features may serve similar functions, they may be related genetically, or they may be linked by processes of growth and development. According to Olson and Miller (1958), all living organisms are composed of these related units, whose degree of relatedness varies based on their relationships to each other and the surrounding environment (Cheverud, 1982). Therefore, a population's phenotype should reflect the relatedness of functionally- and/or developmentally-linked traits (Cheverud, 1982). Additionally, this relatedness should be reflected in the degree of genotypic integration (Cheverud, 1989). Because natural selection occurs at the genetic level, it is these integrated units that evolve by selection instead of individual morphological features. Thus, it is possible then that selection will either act on these individual features as absolutely constrained units that change in synchrony, or they will covary together while retaining some degree of freedom between individual units; the latter is typically what is observed in nature. Thus, it is also possible to approximate the degree of genotype integration using morphological integration (Lande, 1980; Cheverud 1982; Lande and Arnold, 1983). Furthermore, the term morphological integration also refers to patterns of covariation between traits, and can thus be used to describe both a process and a pattern.

At a more basic level, studies of morphological integration can also be used to highlight specific questions related to the existence of correlated features. Analysis of morphological integration within a single species can indicate whether patterns of covariation match predictions related to a single function. Beyond this, analysis of morphological integration among closely related species can be used to identify what factors—function, genetics, and/or development—cause the observed integration for a particular complex of features. If similar patterns of correlation and covariation identified between species where the function of the complex differs, then this pattern is likely the result of genetically- and/or developmentally-determined morphological integration. If, on the other hand, a different pattern of covariation is observed between closely related species where the function of the complex differs, then the observed phenotypic integration pattern is likely to be epigenetically- and/or functionally- determined. Therefore, interspecific studies of morphological integration can be used to evaluate the cause behind observed patterns of covariation. Studies of this kind have been conducted on the skull and face, dentition, and post-crania of mammals including rats and even some primates (Cheverud et al., 1982; Cheverud et al., 1992; Kohn et al., 1993; Ackermann and Cheverud, 2000; Marroig and Cheverud, 2001; Lieberman et al., 2000; Ackermann, 2002; Ackermann, 2004; Grabowski et al., 2011; Lewton, 2012). Thus, studies of morphological integration have been critical for understanding how functional morphological complexes change in response to new functional demands and selective regimes.

Surprisingly, despite the fact that anatomical changes to the foot play a key role in understanding human evolution, especially with regard to the origins of bipedalism, few studies have investigated integration of the foot bones in humans and their closest relatives. Therefore, the goal of this study is to evaluate shape variation of the calcaneus, navicular, and talus among

Homo sapiens, *Gorilla gorilla*, and *Pan troglodytes*. The study's null hypothesis predicts that the calcaneus, navicular, and talus share the same patterns of morphological integration across *H. sapiens*, *G. gorilla*, and *P. troglodytes*.

Morphological integration

Sources of morphological integration

Morphological integration at the genetic level is often the result of pleiotropy, gene duplication, and linkage disequilibrium (Lande, 1980; Cheverud, 1989, Marroig and Cheverud, 2001, Porto et al., 2009), where genes that serve similar purposes with regards to morphological function either become linked or their link is maintained by natural selection. Developmentally-integrated units, on the other hand, result in the covariation of structures due to growth, intercellular interactions, and/or tissue interactions during ontogeny (Zelditch, 1987, 1988). Finally, functionally-integrated units result from similar selective pressures, usually environmentally-based, acting on a series of traits or characters that serve a particular function (Olson and Miller, 1958; Cheverud, 1982, 1989); if traits are functionally linked but not genetically covarying, they may still show a pattern of phenotypic integration in a population. As noted by Zelditch (1988), citing studies of the impact of diet on occlusal surface morphology of teeth, these interactions can have a pronounced effect on patterns of integration. Again, it should be noted that these factors, i.e., genetics, development, and function, are not mutually exclusive and frequently act together to generate morphologically integrated units on which natural selection acts (Olson and Miller, 1958; Cheverud, 1989). Therefore, Marroig and Cheverud (2001: 2577) state that "functional and developmental integration at the individual level leads to genetic integration at the population level, which, in turn, leads to evolutionary integration".

Because of this phenomenon, it is possible to use phenotypic variation as a proxy for genetic variation when examining morphological integration (Marroig and Cheverud, 2001), a task much more feasible for application to the fossil record where genetic material is either absent or highly damaged (Lande, 1980; Cheverud 1982; Lande and Arnold, 1983; Marroig and Cheverud, 2001).

Again, these processes result in the evolution of units that are acted upon as a whole by natural selection (Olson and Miller, 1958; Cheverud, 1982, 1989). Therefore, it would be expected that structures that form a unit are highly integrated whereas independent structures are less integrated (Porto et al., 2009). For example, matching articular surfaces between the bones of a joint should show a high degree of integration with each other either resulting from similar genetic pathways, developmental trajectories that cause the surfaces to match, and/or functional and selective pressures that force genetically and developmentally independent structures to match. In other words, evolutionary forces are unable to cause change in independent structures of perfectly integrated units (Porto et al. 2009). Furthermore, several studies have demonstrated that patterns of morphological integration have remained similar among closely related species, suggesting that the degree and pattern of integration have more to do with phylogeny than environment (Ackermann and Cheverud, 2000; Marroig and Cheverud, 2001; Porto et al., 2009). However, some authors have provided evidence that evolutionary forces can be strong enough to "override" (Porto et al., 2009: 119) patterns of morphological integration brought about by phylogeny. Therefore, the study of morphological integration and its causes and patterns, can help answer a variety of questions about the nature of certain functional units within an organism.

Morphological integration of the postcranial skeleton in primates

Analysis of morphological integration in regions of the post-cranial skeleton are not as common and have primarily focused on the pelvic girdle (Grabowski et al., 2011; Lewton, 2012) and the relationships between the upper and lower limbs (Lawler, 2008; Rolian, 2009; Williams, 2010). These structures have been the focus of such studies because they are highly variable among primates and show varying degrees of modification. Therefore, determining the causes behind this variation, especially in closely related taxa, can shed light on evolution of these morphologically integrated units. In addition, these units have served major roles in the evaluation of the evolution of modern great apes and humans, providing key insights into aspects of biology related to locomotion. Together, these studies have supported Olson and Miller's (1958) hypothesis of morphological integration where traits sharing either common function/development, genetic basis, or evolutionary pressures show higher degrees of covariation than those that do not (Cheverud et al., 1982; Cheverud et al., 1992; Kohn et al., 1993; Ackermann and Cheverud, 2000; Marroig and Cheverud, 2001; Lieberman et al., 2000; Ackermann, 2002; Ackermann, 2004; Lawler, 2008; Rolian, 2009; Williams, 2010; Grabowski et al., 2011; Lewton, 2012). Interestingly, the relationships between the bones of the foot and their articular surfaces have largely gone unexplored in the context of morphological integration, even though the foot also demonstrates high degrees of variation and modification among primates. Differing patterns of integration between species might imply different selective environmental pressures acting via any, or all, of the mechanisms that result in morphological integration, and this could highlight important differences in evolutionary trajectories, especially in a structural unit like the primate foot.

Morphological integration and the foot

The foot is comprised of 26 bones that have been modified across primates as adaptations for different substrates and locomotor behaviors (Day and Wood, 1968; Day and Wood; 1969; Lisowski, 1984; Oxnard, 1980; Latimer et al., 1987; Latimer and Lovejoy, 1989; Sarmiento, 2000; Harcourt-Smith, 2002; DeSilva, 2009; Turley and Frost, 2013; Knigge et al., 2015; Prang, 2015; Prang, 2016). The degree to which this variation is adaptive allows us to study the relationship between morphology and locomotion, which can then be used to study how fossil hominins and apes moved around in the past and what is unique about humans. In particular, the calcaneus, navicular, and talus have been studied extensively individually (Day and Wood, 1968; Lisowski et al., 1974; Latimer et al., 1987; Latimer and Lovejoy, 1989; Gebo, 1992; Sarmiento, 2000; Harcourt-Smith, 2002; Harcourt-Smith and Aiello, 2004; DeSilva, 2009; Turley and Frost, 2013; Prang, 2014; Knigge et al., 2015). However, few studies have evaluated covariation of these bones, though some exist (Turley and Frost, 2014; Prang, 2015; Prang, 2016). Thus, morphological integration studies can inform us about the phenotypic plasticity of these bones as a functional complex, but have yet to be evaluated.

The calcaneus, navicular, and talus function together and are adapted for species-specific substrate use and locomotor behavior. Therefore, selection for change in any of these integrated regions may result in corresponding changes to the other related regions, as one of many phenomena that facilitate selection and evolution of a complex of features (Hallgrimsson et al., 2002; Hallgrimsson et al., 2009; Lewton, 2012). In contrast, functionally unrelated and/or less integrated regions should result in neutral effects of selection and evolution, resulting in less covariation, which could ultimately lead to separate evolutionary and developmental trajectories (Hallgrimsson et al., 2002; Hallgrimsson et al., 2009; Lewton, 2012). The variation observed

among taxa in all three of these bones indicates that if they form a functional unit that varies adaptively, then changes in any one of these bones should be correlated to changes in the others.

Locomotor differences in humans and great apes

Humans and great apes are characterized by different locomotor behaviors. Humans walk almost exclusively bipedally (Aiello and Dean, 1990; Harcourt-Smith, 2002; Harcourt-Smith and Dean, 2004), and are therefore considered specialized for bipedal locomotion. In contrast, the African great apes preferentially move quadrupedally on both terrestrial and arboreal substrates. While the degree and amount of time spent on each substrate varies between species, the African apes demonstrate some major similarities to each other: in a terrestrial environment, the predominant mode of locomotion is quadrupedal knuckle-walking, while in an arboreal environment, quadrupedalism and upright bipedal postures are common, especially in the context of feeding (Elftman and Manter, 1935a; Hunt, 1994; Thorpe et al., 2007). These bouts of arboreal bipedalism, however, are distinct from the human mode in that *Pan* and *Gorilla* adopt a flexed hip and knee posture (also known as a compliant posture) instead of the extended posture seen in humans (Schmitt, 2003; Thorpe et al., 2017). It is important to note that there is a major difference in terrestrial locomotion between *Pan* and *Gorilla*. Generally, *Pan* more commonly uses the flexed stance of bipedal locomotion when foraging from low-hanging branches (Hunt, 1994), whereas *Gorilla* much less frequently exhibits this behavior (Doran, 1997; Thorpe et al., 2007). Another major difference between *Pan* and *Gorilla* is the amount of time spent either arboreally or terrestrially. In general, the larger *Gorilla* species spend more time in terrestrial settings than *Pan* species (Doran, 1997). However, when the animals are similar in size, they spend approximately the same amount of time on the ground or in the trees (Doran, 1997). This

suggests that body size may play a major factor in the substrate use of the great apes (Doran, 1997; Harcourt-Smith, 2002); even within *Gorilla*, there is variation in the proportion of time spent in the trees across species and it has been suggested that body size is a contributing factor to this inter-generic variation as well (Doran, 1997).

Overview of human foot anatomy

The primate foot is composed of 26 bones that can be divided into three major categories, the tarsals, metatarsals, and phalanges. The most posterior portion of the foot, the tarsals, contains seven relatively rectangular bones: the talus, calcaneus, cuboid, navicular, and three cuneiform bones. The intermediate portion of the foot is composed of five metatarsals, long rod-like bones that help form the longitudinal and transverse arches of the human foot. Each of these five metatarsals articulates posteriorly with the tarsals for arch support and anteriorly with a series of phalanges. Anteriorly, the phalanges comprise the five toes of the human foot where each toe possesses three phalanges with the exception of the hallux, or great toe, which only contains two phalanges. The focus of this project is the subtalar joint complex, a joint situated between three of the aforementioned tarsal bones: the calcaneus, navicular, and talus; therefore, these three bones will be the focus of the subsequent discussion.

Calcaneus

The calcaneus is the largest and most robust bone in the foot of both humans and apes since it initially receives all the ground reaction force. Posteriorly, the calcaneus is composed of the calcaneal tuberosity, a large and robust mass of bone while anteriorly, the calcaneal body possesses posterior, middle, and anterior talocalcaneal (Aiello and Dean, 1990). Importantly, the

middle talocalcaneal facet rests on a bony projection for the talar head known as the sustentaculum tali (Aiello and Dean, 1990). The most anterior aspect of the calcaneus contains the cuboid facet for anterior articulation with the cuboid (Aiello and Dean, 1990). In terms of size, the human foot is more robust than that of the African apes. In addition, the human calcaneus possesses an enlarged calcaneal tuberosity whose plantar surface is wide and flattened compared to the calcaneal tuberosity of African apes. In humans, this enlargement is likely the result of the larger Achilles (calcaneal) tendon attachment (Aiello and Dean, 1990). Another stark difference between the human and African ape foot is the calcaneonavicular articulation (Aiello and Dean, 1990). While the African apes retain this articulation, it is completely lost in humans. Furthermore, the cuboid facet of the human foot is asymmetrical where the superior margin extends more anteriorly than the inferior margin, positioning the human cuboid as a keystone of the longitudinal arch and forming a locking mechanism (Aiello and Dean, 1990). In the African apes, however, the cuboid facet is mostly flat and symmetric, and therefore lacks such a locking mechanism (Aiello and Dean, 1990).

Navicular

The navicular is located in the medial portion of the foot where it articulates posteriorly with the talus via a deep concave facet to accommodate the talar head, and anteriorly with the three cuneiform bones (Aiello and Dean, 1990; Harcourt-Smith, 2002). The shape and orientation of the human navicular allows it to assist with arch support of the foot. In addition, the navicular is markedly less wedge-shaped than other extant great apes, contributing to the adducted position of the hallux in humans. The wedge-shape observed in great apes, in

combination with a flatter talar facet, provides the foot with more flexibility and increased range of motion (Aiello and Dean, 1990).

Talus

The talus acts as the link between the foot and the rest of the body by articulating with the tibia superiorly and the calcaneus inferiorly, and thus plays a large role in the functional anatomy of the associated joints. Superiorly, the talus articulates with the tibia via the talar trochlea, a large convex surface on the talar body (Aiello and Dean, 1990). Inferiorly, the talus articulates with the calcaneus at several points comprising the sub-talar joint: the posterior talocalcaneal joint and the anterior and medial talocalcaneal joints (Czerniecki, 1988; Aiello and Dean, 1990). Both the medial and lateral sides of the talus have facets for the medial and lateral malleoli of the tibia and fibula, respectively. Anteriorly, the talar head articulates with the body of the navicular (Aiello and Dean, 1990).

Locomotor differences between the African great apes and humans are reflected in overall talar morphology. The trochlear surface, in conjunction with the small and flattened malleolar facets, forms a locking mechanism that restricts mediolateral movements of the ankle joint in humans. On the other hand, the angled talar surface, and the concave and superiorly oriented malleolar facets of the African great apes facilitates inversion and eversion of the ankle joint, which is important for flexibility on arboreal substrates. Talar head torsion angle may provide a feature of distinction between ape and human tali (Aiello and Dean, 1990). The angle of inclination of the talar neck is distinct in humans and has been suggested to be related to the presence of the longitudinal arch. In addition, the talar neck of the human foot is shorter and wider than that in the African apes. This feature is thought to be associated with the extreme

weight-bearing required by bipedal locomotion on the medial side of the foot (Aiello and Dean, 1990).

Functional morphology and biomechanics of the human and Africa ape

Human foot function in bipedal locomotion

The biomechanics of the human foot have been extensively studied via force plate and footprint analyses, which allow us to understand how force is transmitted through the foot to the rest of the body as well as how each structure of the foot responds to this stress (Czerniecki, 1988). Human bipedal locomotion can be broken down into three major phases: heel strike, stance phase, and toe-off (Czerniecki, 1988). Force plate and footprint analyses demonstrate that, at heel strike, all the ground reaction force is transmitted through the foot via the calcaneal tuberosity (Czerniecki, 1988). Subsequent shifts in body weight promote entrance to stance phase and are accommodated by transmitting the body weight across the lateral longitudinal arch of the foot, supported by the lateral metatarsals, cuneiforms, and cuboid, as the body shifts over the ankle via the talocrural joint (Aiello and Dean, 1990; Harcourt-Smith, 2002; DeSilva, 2010). In humans, the talus forms a locking mechanism with the tibia and fibula to provide stability and allow weight transfer in the anteroposterior direction. More specifically, the trochlear surface of the talus sits parallel to the substrate, where the medial and lateral margins are equal in elevation. This shape provides humans with a large range of motion in the anteroposterior direction while preventing motion in the mediolateral direction (Elftman and Manter, 1935b; Aiello and Dean, 1990). Then, as body weight shifts and the swinging leg begins to drop to the substrate, force is transmitted medially across the planted foot via the medial longitudinal arch and the transverse arch to the medial metatarsal heads and phalanges. This transfer of weight, from lateral to

medial, is permitted by the locked positions of the medial metatarsals and navicular which support the medial longitudinal and transverse arches. Finally, the force of body weight is concentrated on the ball of the foot (the head of the first metatarsal (Aiello and Dean, 1990; Harcourt-Smith, 2002; DeSilva, 2010). Once the swinging leg has entered the heel strike phase, the planted foot enters toe-off, where body weight opposes the ground reaction force to propel the body forward primarily using the great toe (Aiello and Dean, 1990; Harcourt-Smith, 2002; DeSilva, 2010). Throughout this entire cycle, the subtalar joint complex of the human foot is largely involved in generating stiffness and stability in order to create an effective lever arm for efficient weight transfer and toe-off (Aiello and Dean, 1990; Harcourt-Smith, 2002).

Great ape foot & terrestrial locomotion

In contrast to the numerous biomechanical studies conducted on the human foot, few studies have assessed force transmission and gait mechanics in the foot of the great apes (Schmitt, 2003). This is especially true for *Pongo*, with comparatively more studies having been conducted on *Pan* and *Gorilla* foot mechanics (Schmitt, 2003). Unlike humans, the great ape foot never contacts the ground via an exclusive heel strike, resulting in the lack of an expanded and flattened calcaneal tuberosity (Elftman and Manter, 1935a). Instead, the lateral margin of the foot contacts the substrate at the same time as the lateral portion of the heel (Aiello and Dean, 1990; Gebo, 1992). As body weight shifts anteriorly, force is spread across the lateral and medial portions of the foot. During this time, and unlike the human foot, the entire plantar surface of the great ape foot is in contact with the substrate (Elftman and Manter, 1935a; Aiello and Dean, 1990; Gebo, 1992). During the next stage of the gait cycle, entering toe-off, the great ape foot experiences a “midtarsal break” (Elftman and Manter 1935a; Aiello and Dean, 1990), where the

anterior portion of the foot remains completely in contact with the substrate as the heel and tarsus lift. This movement is permitted by the mobility of the tarsometatarsal joint, whose joint surfaces are flat and lack the locking mechanisms that characterize the human tarsometatarsal joint. As a result, the great apes push off from the midfoot rather than the great toe, and thus lack the robusticity of the first metatarsal (Aiello and Dean, 1990; Harcourt-Smith, 2002). Additionally, the length and curvature of the phalanges prevent the efficient toe-off observed in humans. In contrast to the stability provided by the subtalar joint complex in humans, this functional unit in the great apes promotes flexibility. The shapes of the joint surfaces between the calcaneus, navicular, and talus suggest that more movement between bones is permitted in this region to accommodate movement on arboreal substrates and ultimately results in less effective weight transfer and toe in terrestrial locomotion (Harcourt-Smith, 2002).

Great ape foot & arboreal locomotion

Like their behavior on terrestrial substrates, *Pan* and *Gorilla* adopt a plantigrade foot posture on arboreal substrates (Gebo, 1992; Harcourt-Smith, 2002). Therefore, the *Pan* and *Gorilla* foot experiences significant compressive force. When the substrate is small, *Pan* elevates the heel until it can be safely planted on the substrate when it is large enough; contrastingly *Gorilla* rarely travels on small substrates (Gebo, 1992). The grasping function of the great ape foot plays a much larger role on smaller substrates than larger ones and is facilitated by the mobile calcaneonavicular, tarsometatarsal, and metatarsophalangeal joints, especially in the first ray (Harcourt-Smith, 2002). On larger substrates, both *Pan* and *Gorilla* exhibit a style of knuckle-walking like that observed on terrestrial substrates (Gebo, 1992). The African ape foot is equipped to accommodate arboreal substrates by having highly mobile joints and long, curved

phalanges. It is largely the shape of the talar trochlea that determines the range of mobility present in great ape talocrural joint. Compared to humans, this joint forms a "looser" articulation with the medial and lateral malleoli, allowing the ankle to have a greater range of motion in the mediolateral direction, which is also facilitated by the lower elevation of the medial margin of the trochlea compared to the lateral margin (Aiello and Dean, 1990). This configuration and flexibility allows the ape ankle to accommodate movement on arboreal substrates, where inversion and eversion of the foot are crucial (Elftman and Manter, 1935a).

Summary of human and African ape foot biomechanics

Morphological differences observed between humans and extant great apes suggest that the human foot is modified for increased stability, shock absorption, and propulsion to accommodate human obligate bipedalism. The trochlear surface of the talus forms a locking mechanism that restricts motion of the ankle joint to the anteroposterior direction. On the other hand, the angled talar trochlea of great apes facilitates inversion and eversion of the ankle joint, important for flexibility on arboreal substrates. Additionally, the overall morphology of the calcaneus in humans follows the pattern of increased stability while the enlarged calcaneal tuberosity also forms an efficient lever arm for bipedal locomotion. The facet for the cuboid promotes the formation of the longitudinal arches of the foot, which play an important role in shock absorption during bipedal locomotion. Finally, the shape and orientation of the navicular follows the calcaneus, cuboid, and talus in assisting with arch support of the foot. The navicular is markedly less wedge-shaped than other extant great apes, contributing to the adducted position of the hallux in humans. Together, these differences result in a foot structure functionally adapted for bipedal locomotion.

Research questions

Analysis of morphological integration can be broken down into two categories: examination of patterns of covariation and integration within species and patterns of integration between species. Patterns of covariation and integration within species should mirror the differing biomechanical demands of articular and non-articular surfaces within each bone. Therefore, I expect that within species, within bone patterns of correlation are expected to be greater between articular surfaces than non-articular surfaces for the calcaneus, navicular and talus, since these surfaces should be related to adaptive function. Additionally, differing locomotor behaviors exhibit different biomechanical and functional demands on the subtalar joints of African apes and humans. Thus, between species, it is expected that the pattern of integration will differ due to differing locomotor demands of *Homo sapiens*, *Gorilla gorilla*, and *Pan troglodytes*.

Chapter 2 Materials and Methods

Data collection

Data were collected from the Hamann-Todd Collection at the Cleveland Museum of Natural History. Calipers were used to collect linear measurements that have been defined by previous studies (Gebo and Schwartz, 2006; Prang, 2014; Sarmiento and Marcus, 2000; Seiffert and Simons, 2000; Zipfel et al, 2011). The data for this study includes linear measurements from the talus, calcaneus, and navicular of 12 *Homo sapiens*, 12 *Gorilla gorilla*, and 11 *Pan troglodytes*. Measurements were taken from both the left and right foot, where possible. A total of 20 measurements were taken for the talus, 16 for the calcaneus, and 11 for the navicular (Tables 1-3). Additionally, articular surface areas, calculated using the formula for area of a rectangle and corresponding linear measurements, and the geometric mean of each bone using all variables were calculated in Microsoft Excel (Tables 1-3). All specimens were randomly selected adults (determined by collected information), and an effort was made to sample equal numbers of males and females. However, equal sampling of the sexes was not achieved and this could cause problems in the data analysis. For example, all *H. sapiens* specimens are male, all but two *G. gorilla* specimens are male, and three of the *P. troglodytes* specimens are male. Because of this unequal sampling, sexes were pooled for all analyses.

Statistical analysis

Analysis of shape variation and covariation

To evaluate how each bone for each species differs in shape, principal components analyses of the variance/covariance matrices for the size-adjusted data were conducted in PAST (Hammer et al., 2001) and was bootstrapped 1000 times to account for small sample size. The

results of these analyses for each bone were used to identify which variables load on the relevant PC axes most heavily. Relevant PC axes were defined as those that account for more than five percent of the observed variance, and the cut-off point for PC loadings was set to the absolute value of 0.2; this value was selected as the cut-off point because all values below this dropped off dramatically.

For all analyses, the critical α was set at 0.05. A multivariate analysis of variance (MANOVA) was conducted in PAST (Hammer et al., 2001) to examine differences in group means when scaled by the geometric mean. The results of the MANOVA analyses were used to further refine subsequent analyses by eliminating variables that whose groups means were not significantly different to focus analysis on just those variables that show differing relationships between taxa. Finally, a one-way analysis of variance (ANOVA) was conducted for each of the most important shape variables to examine differences in group means. For each variable, a Levene's test was performed to test for homogeneity of variance. When this assumption was not met, a Welch's test was used instead of the classic one-way ANOVA model (Field, 2013). A Bonferroni post-hoc test was used to examine pairwise differences between groups for each of these variables (Field, 2013).

Analysis of morphological integration

In order to detect patterns of morphological integration both within and between bones of each species, correlation matrices were generated in IBM SPSS (IBM Corp, 2013) and the Pearson correlation coefficients were plotted in Microsoft Excel to visualize any patterns that may be present within and between bones of each species (Microsoft, 2016). In addition, principal component analyses based on the correlation matrices were generated for each bone

using PAST (Hammer et al., 2001) to examine relationships between species and to evaluate which bony features best separate taxa. A factor analysis of the correlation matrix for each bone was conducted in SYSTAT V.13 to examine patterns and relationships between species and to further identify which bony features best distinguish taxa. Finally, SYSTAT V.13 was used to generate correlation matrices for each bone of each taxon, and Microsoft Excel (Microsoft, 2016) was used to calculate the median positivized correlation coefficients for between articular surfaces, between non-articular surfaces, and between articular and non-articular surfaces of each bone for each taxon in order to examine the magnitude of overall patterns of correlation within each bone.

Chapter 3 Results

Shape variation and covariation

Calcaneus

The PCA of the scaled data reveals that PC1 and PC2 account for 71.21% and 28.51% of variance, respectively. However, examination of the scatter plot shows very poor separation between taxa along both axes (Figure 1). Talar articular surface area and cuboid facet area contribute most to the loadings of each axis (Table S1). Therefore, these variables were used for all subsequent analyses.

Comparison of group means using MANOVA revealed that, when adjusted by geometric mean, groups means of these shape variables are significantly different (Wilk's $\lambda = 0.00476$, $F_{(36,80)} = 29.24$, $p < 0.001$) (Table 4). Additionally, Bonferroni-corrected *p*-values for multiple comparisons demonstrate that all groups are significantly different from one another ($p < 0.001$). Comparison of group means using one-way ANOVA (Table 5) demonstrates that species clearly differ in means of talar surface area and cuboid facet area ($p < 0.001$), where *post hoc* Bonferroni multiple comparisons tests reveal that all three groups are significantly different from one another ($p < 0.05$) (Table 6).

Navicular

The PCA model for the scaled navicular linear measurements demonstrates that the first three PC axes represent the majority of variance within the sample, where PC1 accounts for 76.6%, PC2 for 18.51%, and PC3 for 4.75%. For the first component axis, *P. troglodytes* separates relatively well from *H. sapiens* and *G. gorilla*, but there appears to be poor separation of *H. sapiens* and *G. gorilla* for each of these subsequent components (Figure 2). The variables

that load on these components most strongly include all of the articular surface areas on the navicular, such as those for the cuboid, talus, and three cuneiforms (Table S2). Therefore, these variables were used for all subsequent analyses.

Comparison of group means using MANOVA revealed that, when adjusted by geometric mean, groups means of these shape variables are significantly different (Wilk's lambda = 0.0156, $F_{(32,84)} = 18.39$, $p < 0.001$) (Table 4). Additionally, Bonferroni-corrected p-values for multiple comparisons demonstrate that all groups are significantly different from one another ($p < 0.001$) (Table 7). Finally, one-way ANOVA of groups means for talar facet area revealed that groups are statistically significantly different ($F_{(2)} = 49.126$, $p < 0.001$) (Table 5). The *post hoc* Bonferroni multiple comparisons test (Table 8) revealed that while *H. sapiens* and *G. gorilla* groups means are not significantly different from one another whereas all other species pairings are ($p < 0.001$).

Talus

The PCA model on the linear talar measurements shows that the first three PC axes represent most variance within the sample, 76.7%, 18.5%, and 4.8%, respectively. For the first component, *P. troglodytes* separates relatively well from *H. sapiens* and *G. gorilla*, but there appears to be poor separation of *H. sapiens* and *G. gorilla* for each of the subsequent components (Figure 3). The variables loading each component most heavily include talar head area, plantar facet area, and plantar facet length (Table S3). Therefore, the variables used for further analysis were based on those shown to be most heavily loading from the scaled PCA: talar head area, plantar facet area, and plantar facet length.

Comparison of group means using MANOVA revealed that, when adjusted by geometric mean, groups means of these shape variables are significantly different (Wilk's lambda = 0.004319, $F_{(44,74)} = 23.91$, $p < 0.001$) (Table 4). Additionally, Bonferroni-corrected p-values for multiple comparisons demonstrate that all groups are significantly different from one another ($p < 0.001$) (Table 9). Finally, one-way ANOVA analysis of groups means for talar head area reveals that groups are statistically significantly different (Table 5). The *post hoc* Bonferroni multiple comparisons test (Table 10) reveals that while *H. sapiens* and *G. gorilla*, and *H. sapiens* and *P. troglodytes* groups means are significantly different from one another ($p < 0.001$), *G. gorilla* and *P. troglodytes* are not significantly different from one another ($p = 0.18$).

Morphological integration

Within species patterns of correlation

Visualizations of the Pearson correlation coefficients for comparison within and between bones revealed minimal degrees of correlation, at best. Preliminary results show no general difference in the magnitude of correlations within and between bone articular surfaces and non-articular features (Figures 4-9). Together, these figures (Figures 4-9) demonstrate that there is no clear pattern of correlation within or between bones for each species. However, PCA analyses for the correlation matrices of the calcaneus, talus, and navicular revealed that there is some patterning present that separates *H. sapiens* from *P. troglodytes* and *G. gorilla* along components 1 and 2 for each bone (Figure 10); other principal component axes lack meaningful separation between taxa.

Calcaneus. The PCA loadings based on the correlation matrices of the calcaneus for each taxon are presented in Table S4. Overall, there seem to be few commonalities between taxa in terms of the variables that contribute most strongly to either the positive or negative ends of each PC axis. The cut-off point for the relevant loadings were determined based on where the magnitude dropped-off dramatically. Based on these loading scores, it appears as though most commonalities observed are those shared by *H. sapiens* and *G. gorilla*, although some exist between all three and others exist between *G. gorilla* and *P. troglodytes*, and *P. troglodytes* and *H. sapiens*. For example, mediolateral tuberosity width is common to all taxa, strongly loading at the negative end of PC1.

Alternatively, the factor analysis based on the correlations matrices of the calcaneus for each taxon show very few, if any, common patterns between taxa (Table S5). Only mediolateral tuberosity width at the peroneal trochlea is common to loading all three taxa on the negative end of factor 1. For all other factors, there are no shared measurements that load the axes in either direction for any taxa.

Navicular. The PCA loadings based on the correlation matrices of the navicular for each taxon are presented in Table S6. Unlike the calcaneus, more patterns of similarity are observed between taxa for the navicular. For example, all three taxa share talar facet minor axis diameter as a common measurement driving variation toward the negative end of PC1. Similarly, *H. sapiens* and *G. gorilla* share cuboid facet area (CFA) and cuboid facet dorsoplantar diameter at the positive end of PC2. For PC3, all taxa are most heavily loaded by mesocuneiform facet mediolateral diameter on the positive end, where other similarities are shared between *H. sapiens* and *G. gorilla*, *G. gorilla* and *P. troglodytes*, and *H. sapiens* and *P. troglodytes*. Similar patterns

are observed for the other PC axes as well, with various combinations of shared patterns between taxa.

The opposite case appears to be true for the factor analysis of the navicular correlation matrices for each taxon (Table S7). Few measurements load commonly among taxa. While a few, such as cuboid facet dorsoplantar diameter, cuboid facet mediolateral diameter, and cuboid facet area (CFA) contribute to most of the variation on the positive end of factor 2, are shared by *H. sapiens* and *G. gorilla*, most other commonalities between taxa for the remaining factors occur between *H. sapiens* and *P. troglodytes* or *G. gorilla* and *P. troglodytes*, if they exist at all.

Talus. The PCA loadings based on the correlation matrices of the talus for each taxon are presented in Table S8. Commonalities between taxa are marginal best. While all three taxa share lateral body height, anterior trochlear width, and posterior trochlear width as measurements that drive the positive loading along PC1, other patterns of shared measurements are variable and heavily loaded measurements are shared between all possible combinations of taxa for each PC axis. A similar phenomenon is apparent for the factor analysis as well (Table S9). Therefore, unlike the results of these analyses for the calcaneus and navicular, common patterns observed for the talus are tentative, and there is no clear association between specific groups of measurements between taxa.

Summary of PCA and factor analysis results

Results of the factor analysis, which allows rotational freedom of the axes, corroborated the results generated from the correlation matrix PCA. For all bones, only factors 1 and 2 successfully separated taxa into clear groupings (Figure 11). The variables that drive separation

are listed in Tables S10-S12. In general, the PCA and factor analyses use the same measurements to distinguish between taxa, where those related to articular surfaces were used most frequently.

Within bone patterns of integration

The median values for the Pearson correlation coefficients, calculated within each bone according to the aforementioned pairings (i.e., between articular surfaces, between non-articular surfaces, and between articular and non-articular surfaces), demonstrate that within each species there is no evident pattern of integration between any of the pairings (Table 11). This pattern, or lack thereof, holds across all three taxa for each bone studied. Where slight differences in median correlation do exist, it cannot at this time be determined if this reflects a true pattern or is an effect of small sample size.

In summary, the overall magnitude of correlations is relatively low (Table 11), though some features did show very high correlations (Figures 4-9, 11). Factor analysis (Figure 11) clearly separates humans, gorillas and chimpanzees, as expected, but the pattern of loadings could not be clearly matched to the pattern of within-species correlations. However, plotting arrays of within-species correlations against one another suggests that species share similar patterns of correlations for each bone (Figure 12); this observation holds true across taxa for all three bones. Interestingly, articular surface dimensions consistently show positive correlations in these comparisons. However, at this time it cannot be determined which specific shape variables are driving these patterns due to small sample sizes.

Chapter 4 Conclusion and Discussion

Shape variation and covariation

The most important variables for loadings of shape variation in the calcaneus PCA were talar articular surface area and cuboid facet area. Analysis of these shape variables using the MANOVA model demonstrates that taxa group means are significantly different. Results of the one-way ANOVA of talar articular surface area and cuboid facet area demonstrate that group means are significantly different, where all three species (*H. sapiens*, *G. gorilla*, and *P. troglodytes*) are significantly different from one another. Two additional variables that demonstrate differences in species are neighboring joint surfaces between the navicular and talus (talar facet area and talar head area, respectively). The *post hoc* Bonferroni comparisons show differences about which groups are statistically different from one another in each case. Therefore, talar facet area is probably a good proxy to use when examining differences in shape variation between *H. sapiens* and *P. troglodytes*, and *G. gorilla* and *P. troglodytes*; however, it is not advisable to use talar facet area to distinguish between *H. sapiens* and *G. gorilla*, since species means are not significantly different. On the other hand, talar head area is probably a good proxy to use when examining differences in shape variation between *H. sapiens* and *G. gorilla*, and *H. sapiens* and *P. troglodytes*; however, it is not advisable to use talar head area to distinguish between *G. gorilla* and *P. troglodytes* since species means are not significantly different.

The primary goal of this study was to evaluate which measurements separate species to see if any pattern in differences of locomotory behavior can be recognized. The results demonstrate that the variables that best separate species are talar articular surface area and

cuboid facet area on the calcaneus, talar facet area of the navicular, and talar head area of the talus. This is interesting because these variables are all articular surfaces and together are associated with mobility of the foot, and could thus be associated with differences in locomotor behavior (Aiello and Dean, 1990; Harcourt-Smith, 2002; Harcourt-Smith and Aiello, 2004). In modern humans, the joints formed by these surfaces are associated with supporting the longitudinal arches of the foot, whereas these joints are associated with foot mobility in *P. troglodytes* and *G. gorilla* (Aiello and Dean, 1990; Harcourt-Smith, 2002; Harcourt-Smith and Aiello, 2004). Joint stability and arch support occurs in humans as a response to bipedal locomotion, while joint mobility in great apes helps accommodate foot positioning on branches in arboreal locomotion (Aiello and Dean, 1990; Harcourt-Smith, 2002; Harcourt-Smith and Aiello, 2004), so it is not surprising that species differ in these surfaces.

Morphological integration

Results of the correlation and integration analyses suggest that while species can be grouped based on variables related to articular surface morphology, especially with respect to the joint between the navicular and talus, overall differences in patterns of morphological integration are minimal. Pearson correlation coefficients, based on the correlation matrices, demonstrated that there was no substantial difference between species in terms of patterns of morphological integration when comparing within bone to between bone data. This could indicate that all taxa examined, *H. sapiens*, *G. gorilla*, and *P. troglodytes*, have very loosely integrated foot morphology which would allow for the evolution of the major differences related to varying locomotor behaviors, such as a more flexible or more restricted subtalar joint. Furthermore, any differences that are demonstrated by the patterning of the Pearson correlation coefficients were

detected by the PCA and factor analysis. For both analyses, only the first two axes successfully separated taxa and the variables that best account for these differences are related to articular surface measurements. Therefore, the analysis of shape variation/covariation, in conjunction with analysis of morphological integration, suggest that articular surface shape could potentially be used to distinguish between *H. sapiens*, *G. gorilla*, and *P. troglodytes*, where patterns of integration among these articular surfaces are loose enough, because overall patterns of correlation are low, to be able evolve in correspondence with differing locomotor modes. This result is similar to that presented by Grabowski et al. (2011) and Williams (2010). Just as patterns of morphological integration were most variable in regions of the hip (Grabowski et al., 2011) and wrist (Williams, 2010) associated with locomotor behavior, here too the subtalar joint surfaces show less integration within and between bones, resulting in less constraint on morphology of the foot in the evolution of bipedal locomotion in humans. While at this time it cannot be definitively determined which articular surfaces of the calcaneus, navicular, and talus are driving these patterns of loose integration, it is likely that the talonavicular joint is a contributing factor because its provides stability to the human subtalar joint (Aiello and Dean, 1990; Harcourt-Smith, 2002; Harcourt-Smith and Aiello, 2004) and was able to separate taxa in the aforementioned shape variation analyses.

However, analyses of morphological integration suggest that there are no general patterns of integration distinguishing articular surfaces from non-articular parts of the bones in any taxa. These results suggest two possibilities: either the bones of the foot are loosely integrated and facilitate evolutionary modification, or the sample size is too small to detect true patterns of integration. It is interesting that these results demonstrate no pattern difference between humans and African great apes because similar results have been found in morphological integration

studies of the wrist (Williams, 2010), where the magnitude and pattern of integration were not unique among knuckle-walkers like chimpanzees and gorillas. Instead, the magnitude and pattern of integration within the wrist were similar between African great apes and humans, even though humans are not knuckle-walkers (Williams, 2010). This lack of unique patterning in the human subtalar joint could suggest that this joint does not constitute a functional complex, as Williams (2010) has suggested for the African great ape and human wrist. The pattern of correlation is itself correlated consistently across species for each bone (Table 11), with correlations among measurements of articular surfaces consistently positive (Figure 12). This suggests that at the least there are shared patterns of integration across species in the articular surfaces, again demonstrating that the human subtalar joint is not unique in terms of pattern of morphological integration. Again, this finding corroborates the idea that the subtalar joint does not form a functional complex and should not be used as such in cladistics analyses (Williams, 2010). However, the small sample size of this study may be obscuring more subtle pattern differences that suggest otherwise. Thus, if there are patterns of integration, then larger sample sizes will be needed to detect patterns of integration and elucidate which shape variables are driving these patterns. It is surprising and intriguing, however, that any common patterns have been demonstrated at all given these limitations, and future work will continue to resolve and refine the analysis presented here.

In sum, within species locomotor behavior, at least between articular surfaces, does not appear to drive patterns of integration within the subtalar joint. On the other hand, humans, gorillas, and chimpanzees do share similar patterns of integration within each one of the bones. This could mean two things: either that some degree of constraint is limiting the degree of modification allowed throughout evolution, or that the patterns of integration themselves are

fluid enough to allow modification for adequate functional variation. Unfortunately, it is unclear at this time which of these drives the differences observed in the human and African great ape foot. What can be concluded, though, is that patterns of integration are not different between species, so differences in human foot anatomy are not constrained by ancestry, i.e., the human foot evolved within the pattern of integration that likely already existed. Therefore, the modifications of the subtalar joint in humans could be a function of differing biomechanical demands related to bipedalism. A study focusing on the ontogeny of the talocrural joint (Turley and Frost, 2014) demonstrated that substrate use significantly impacts the shape of this joint. Though this sort of study has yet to be conducted on the subtalar joint, one could hypothesize that a similar phenomenon maybe be at play. Because patterns of integration are not different between the taxa examined here, differences in subtalar joint morphology could be attributed to differences in substrate use related to locomotor behavior and developmental plasticity (Elftman and Manter, 1935a; Gebo, 1992; Aiello and Dean, 1990; Harcourt-Smith, 2002) rather than differing evolutionary selection pressures and evolutionary integration (Zelditch, 1987, 1988). These biomechanical and functional demands would have acted on a foot that could just as easily become that of an African ape due to shared patterns of integration. Because the African apes and humans share similar patterns of integration, any biomechanical or functional demand that differs between taxa would have resulted in corresponding changes in foot structure, probably throughout ontogeny, but without altering the degree or pattern of morphological integration. Other processes associated with genetic integration, such as gene linkage and duplication (Lande, 1980; Cheverud, 1989, Marroig and Cheverud, 2001, Porto et al., 2009), could have transformed these epigenetic pressures into heritable characteristics (Marroig and Cheverud, 2001) that result in the differences observed today between human and African great ape subtalar morphology.

Limitations and future directions

While the results of this study suggest that there are no morphological integration pattern differences of the subtalar joint between African great apes and humans, this study was conducted on a very small sample size, where only 12 humans and gorillas, and 11 chimps were examined. This sample size is simply too small to truly detect reliable patterns of covariation and integration considering most studies of this sort include hundreds of individuals from several species (Grabowski and Porto, 2016). Additionally, unequal sampling of sexes may confound the results presented. While it is unclear whether sexual dimorphism plays a role in the morphological integration of the foot, differences in degree of sexual dimorphism could contribute to the observed patterns. Thus, the results presented here are tentative but intriguing.

To overcome these limitations, future analyses of morphological integration of the subtalar joint should incorporate larger samples with wider phylogenetic diversity and locomotor behaviors to better detect patterns of covariation and integration within and between species. Additionally, more refined analyses of integration, could help shed light on the degree of relatedness between patterns of integration, function, and phylogeny. Furthermore, future analyses should examine which specific shape variables seem to contribute most strongly to the observed patterns of integration between species to identify which aspects of foot morphology are most susceptible to forces of evolutionary change, such as functional and biomechanical demands. Examination of the developmental pathways leading to the formation of the subtalar joint and whether these observed patterns of integration could be a result of developmental integration is another worthwhile pursuit in evaluating the evolution of bipedal locomotion. Furthermore, an examination of the genetic control of foot development to identify the genes

involved for each species and whether these are linked to one another in some way, and if so, is this linkage the same across species.

Figures and Tables

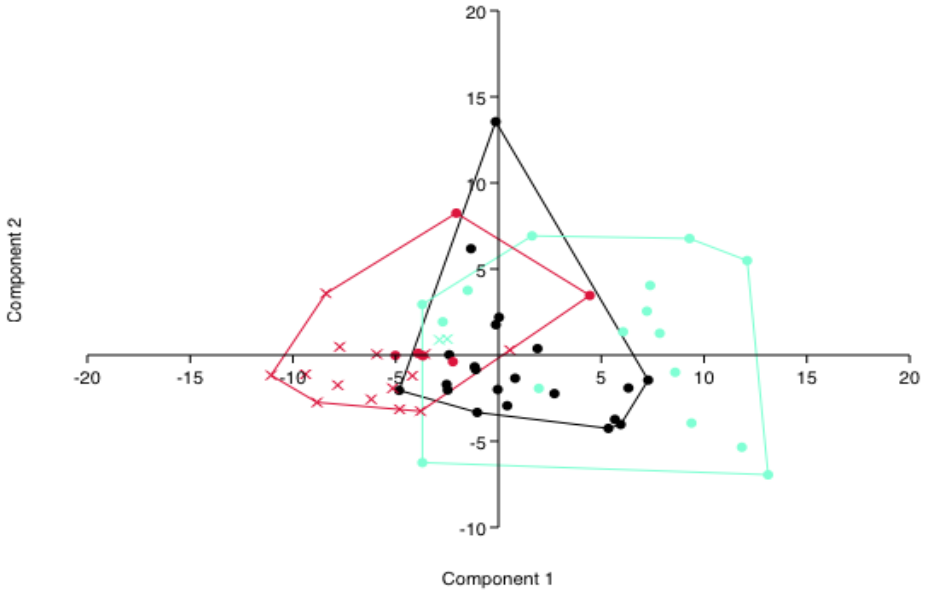

Figure 1. Plot of PC1 and PC2 for the scaled calcaneus data. Red = *P. troglodytes*, black = *H. sapiens*, blue = *G. gorilla*; x = female, dot = male.

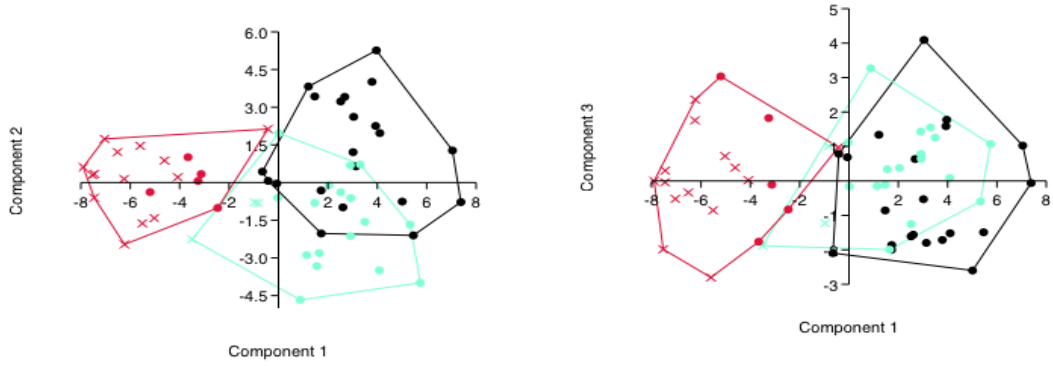

Figure 2. Plots of PC axes 2-3 against PC axis 1 for the scaled navicular data. Red = *P. troglodytes*, black = *H. sapiens*, blue = *G. gorilla*; x = female, dot = male.

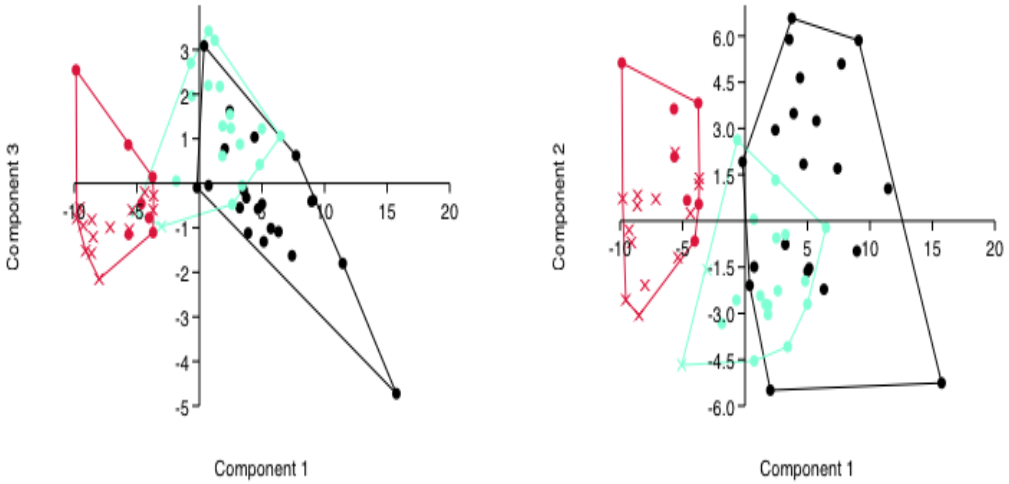

Figure 3. Plots of PC axes 2-3 against PC axis 1 for the scaled navicular data. Red = *P. troglodytes*, black = *H. sapiens*, blue = *G. gorilla*; x = female, dot = male.

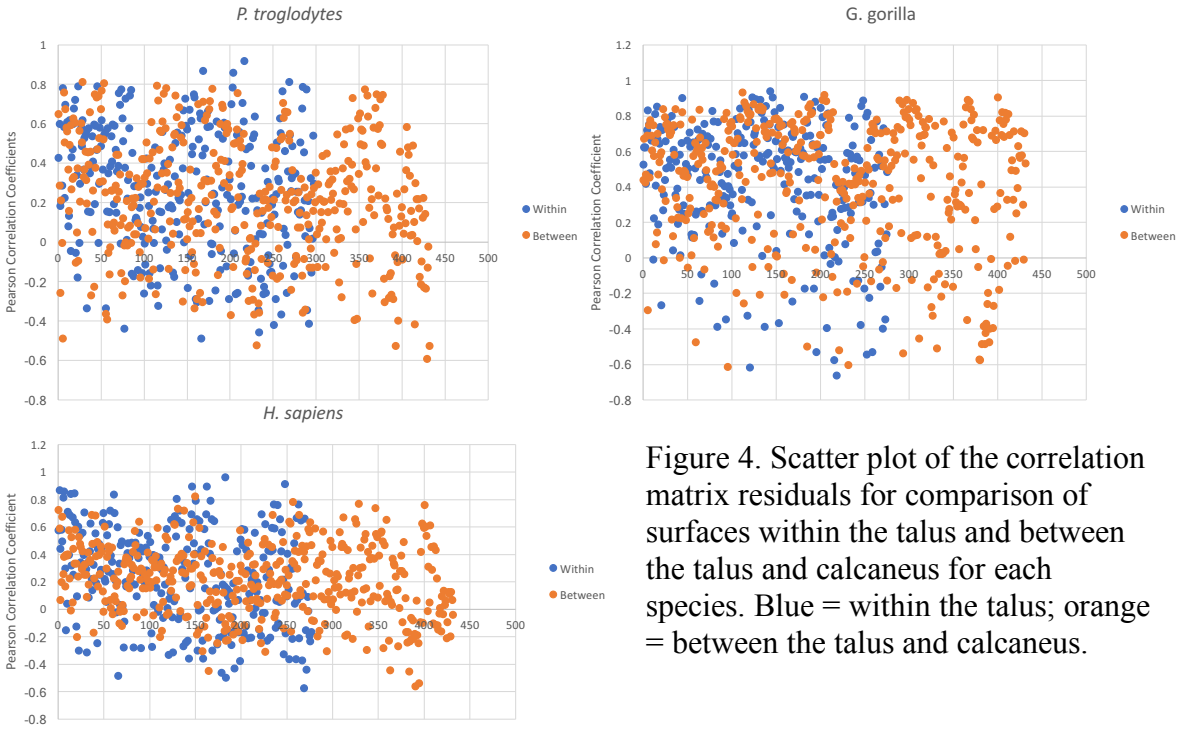

Figure 4. Scatter plot of the correlation matrix residuals for comparison of surfaces within the talus and between the talus and calcaneus for each species. Blue = within the talus; orange = between the talus and calcaneus.

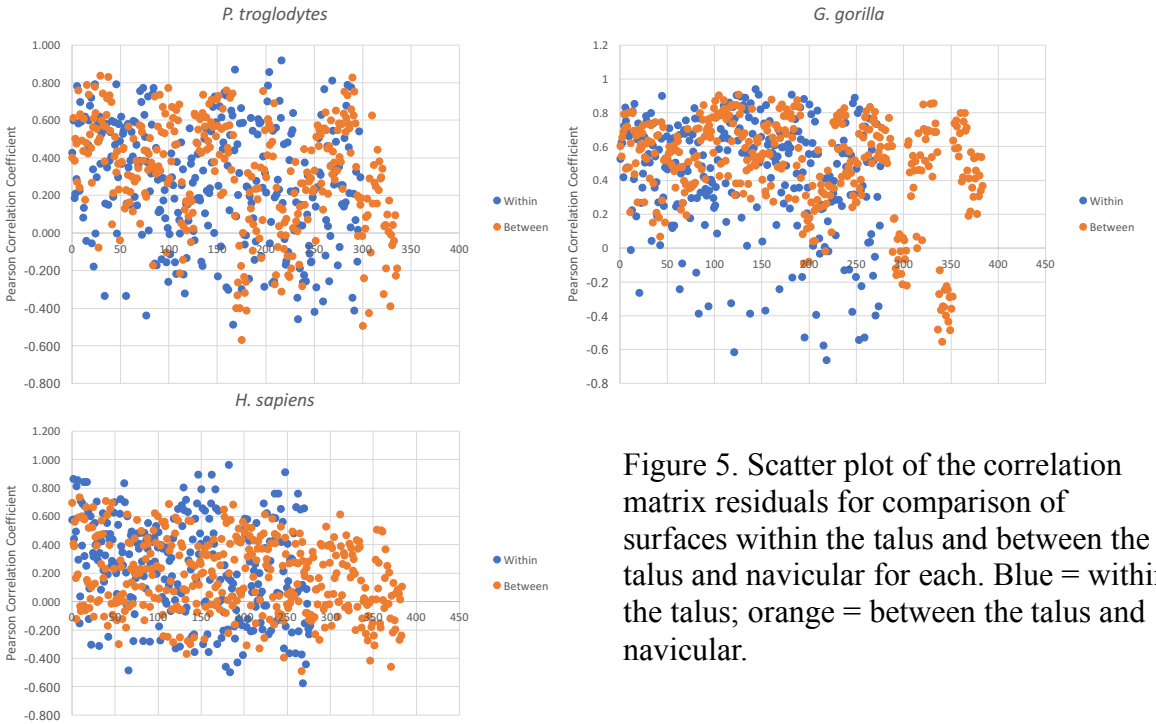

Figure 5. Scatter plot of the correlation matrix residuals for comparison of surfaces within the talus and between the talus and navicular for each. Blue = within the talus; orange = between the talus and navicular.

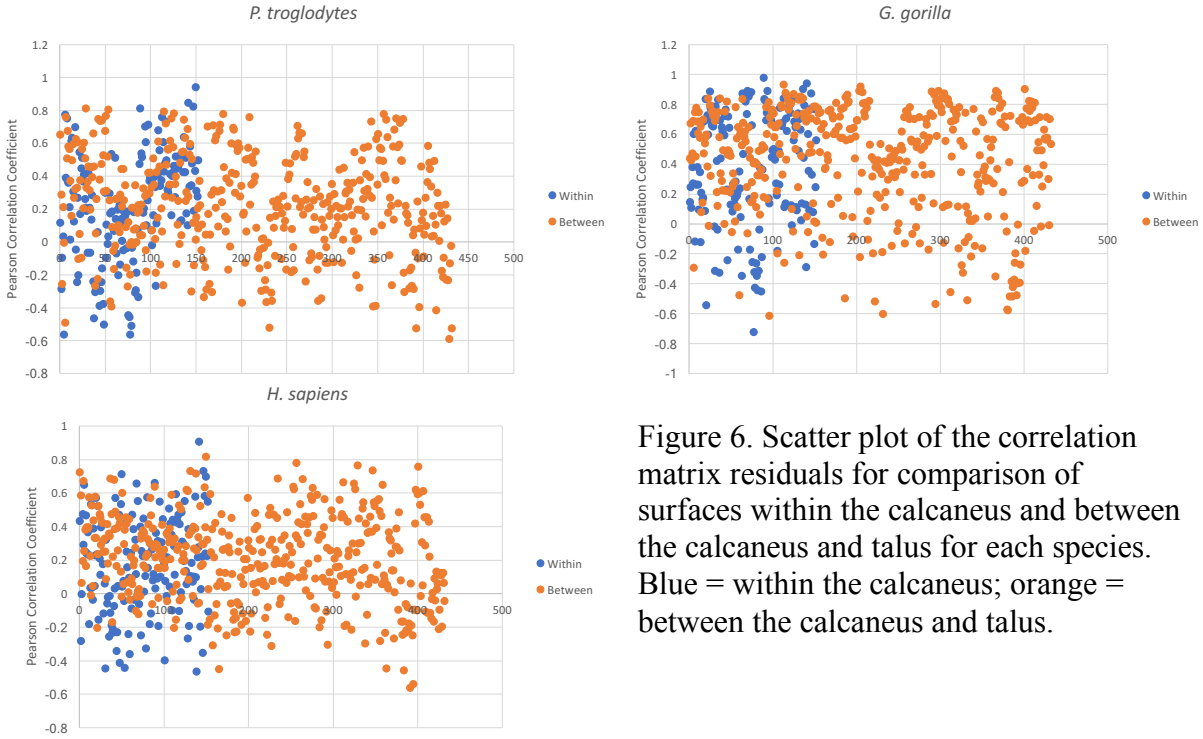

Figure 6. Scatter plot of the correlation matrix residuals for comparison of surfaces within the calcaneus and between the calcaneus and talus for each species. Blue = within the calcaneus; orange = between the calcaneus and talus.

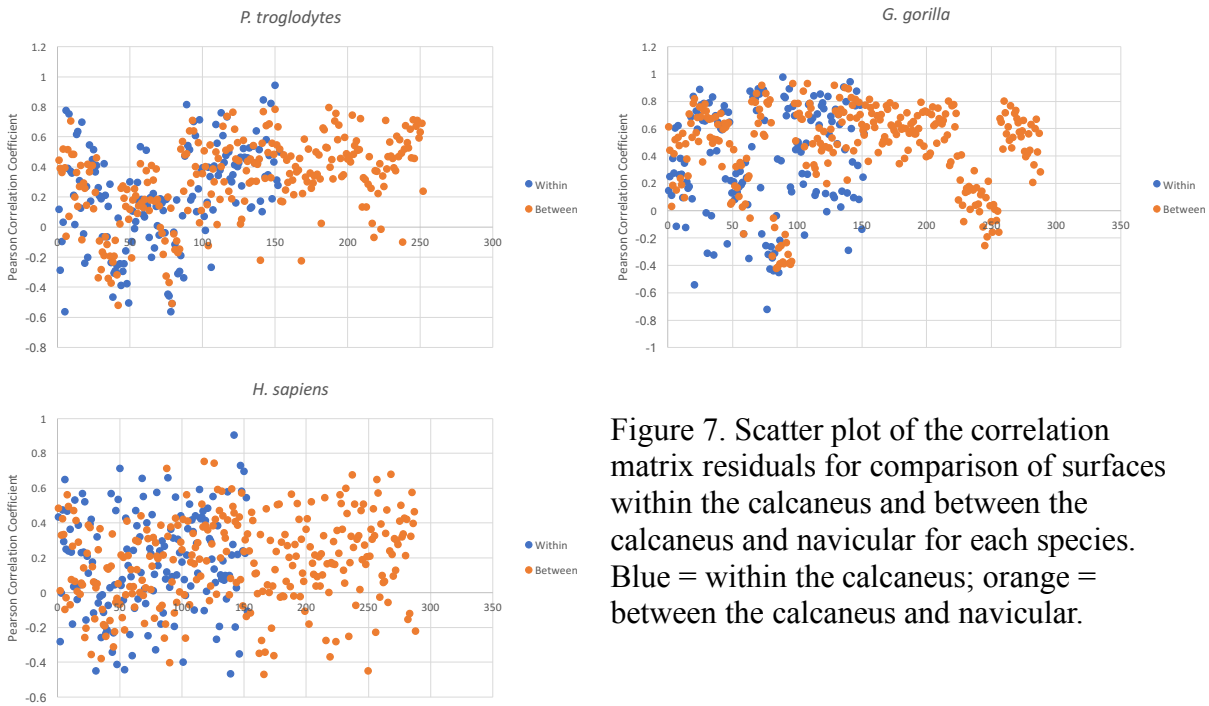

Figure 7. Scatter plot of the correlation matrix residuals for comparison of surfaces within the calcaneus and between the calcaneus and navicular for each species. Blue = within the calcaneus; orange = between the calcaneus and navicular.

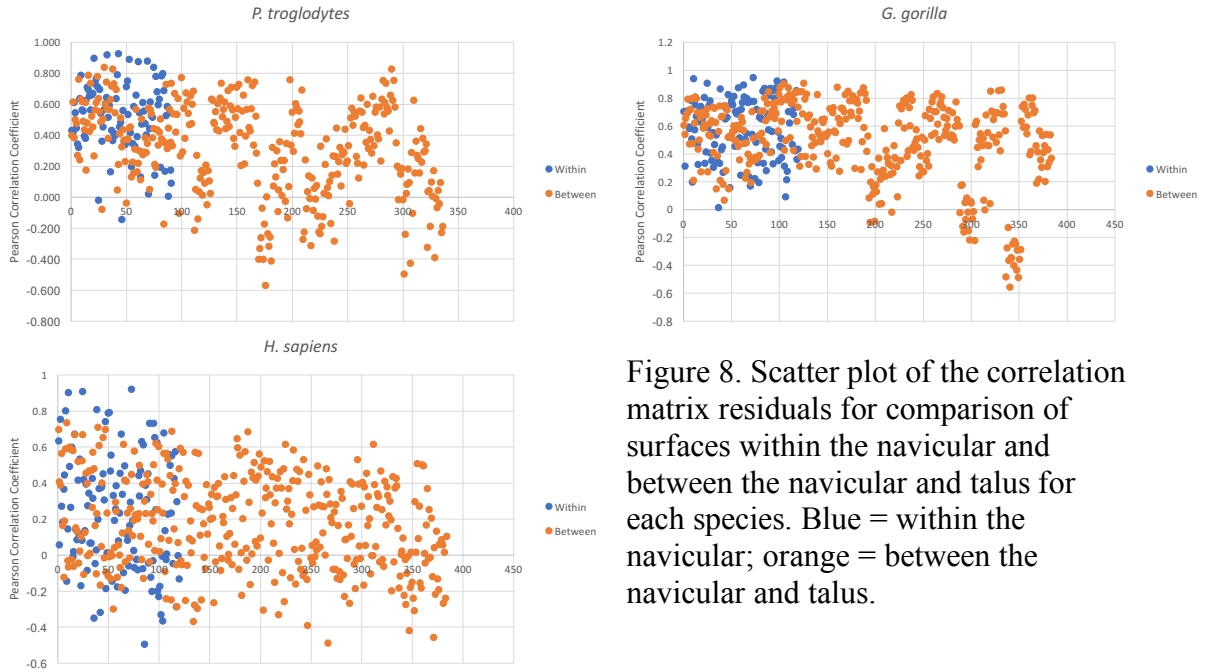

Figure 8. Scatter plot of the correlation matrix residuals for comparison of surfaces within the navicular and between the navicular and talus for each species. Blue = within the navicular; orange = between the navicular and talus.

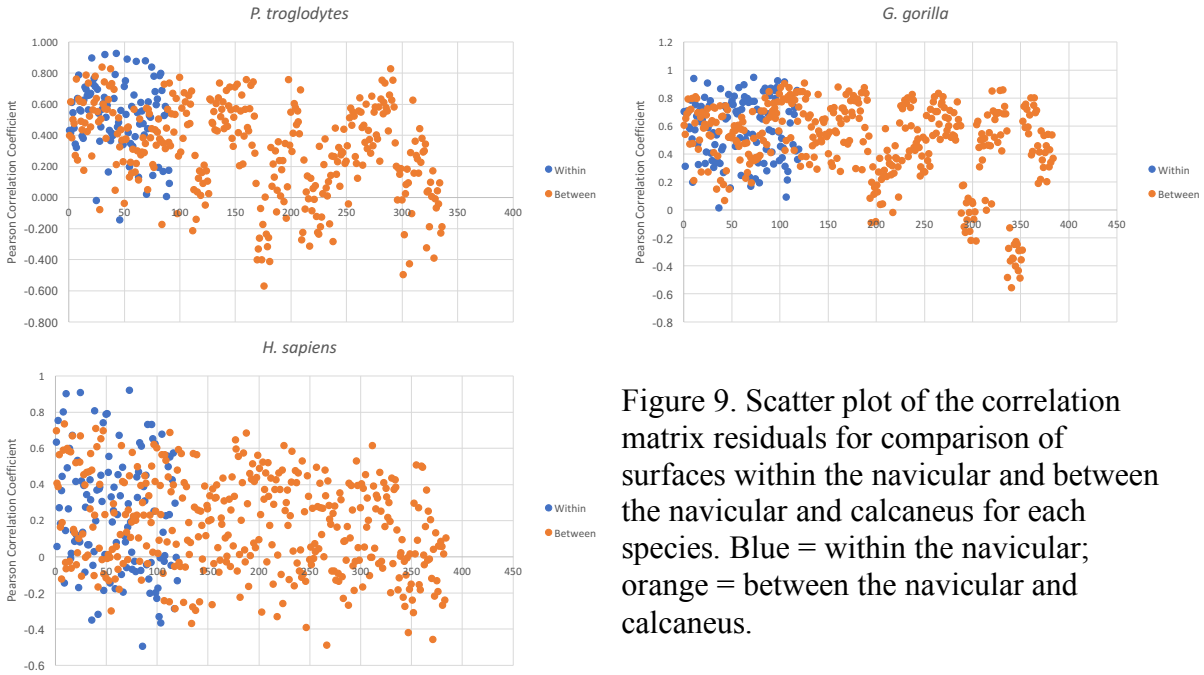

Figure 9. Scatter plot of the correlation matrix residuals for comparison of surfaces within the navicular and between the navicular and calcaneus for each species. Blue = within the navicular; orange = between the navicular and calcaneus.

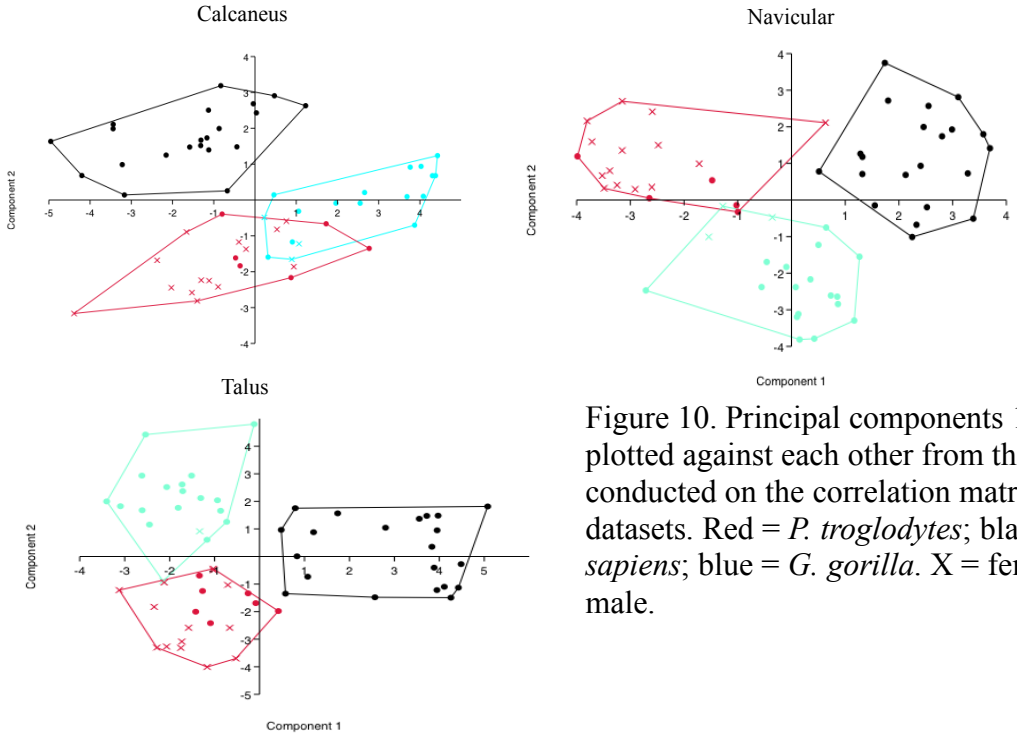

Figure 10. Principal components 1 and 2 plotted against each other from the PCA conducted on the correlation matrices of the datasets. Red = *P. troglodytes*; black = *H. sapiens*; blue = *G. gorilla*. X = female; dot = male.

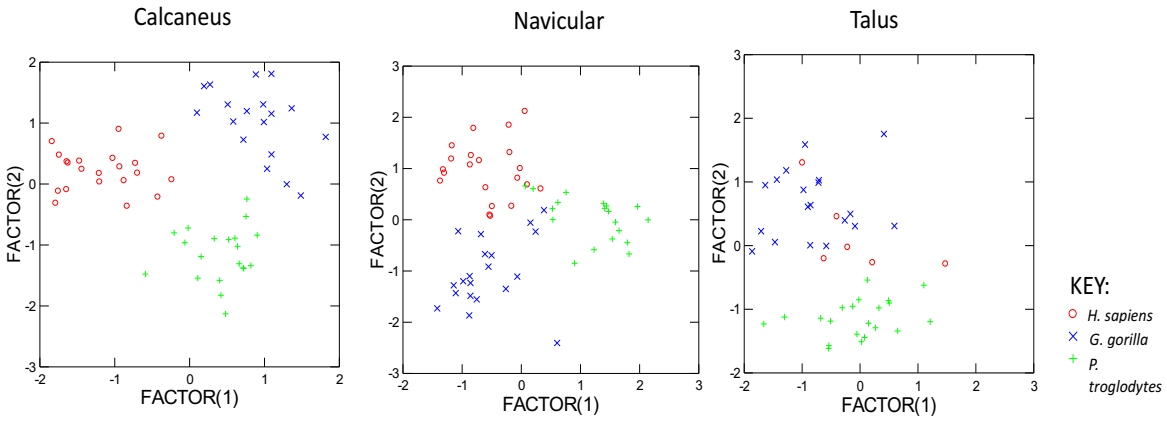

Figure 11. Results of the factor analysis based on the correlation matrix generated from all measurements, scaled by geometric mean, for each bone. Only factors 1 and 2 and shown because these best separated taxa, while other factors demonstrated poor separation. Red dot = *H. sapiens*, blue x = *G. gorilla*, green + = *P. troglodytes*.

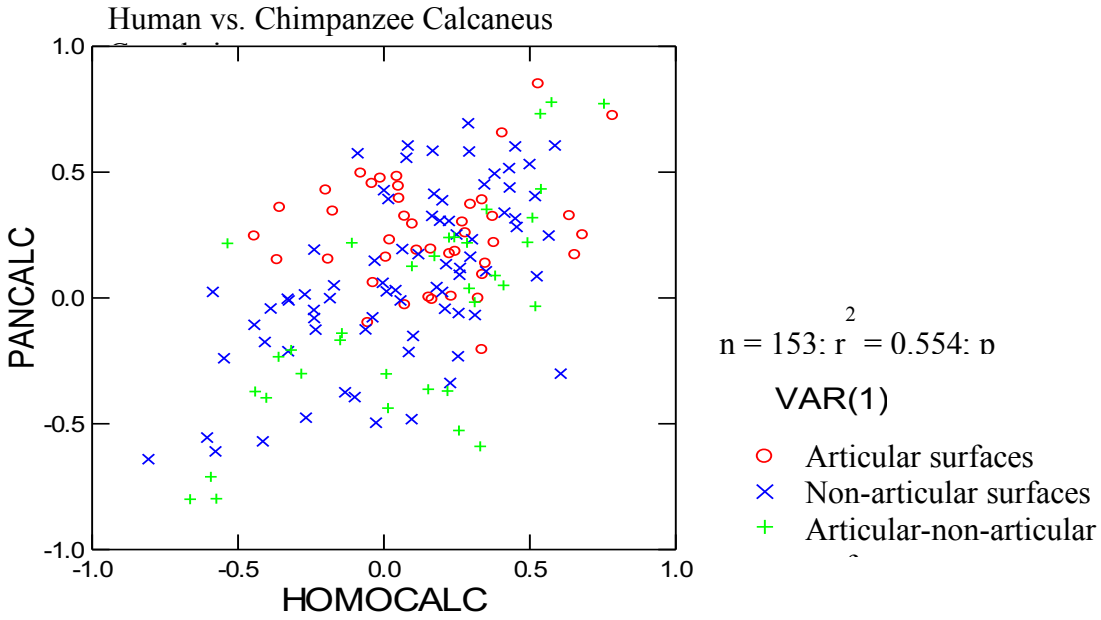

Figure 12. Plot of arrays of within-species correlations comparing the human calcaneus to the chimpanzee calcaneus. Articular surfaces (red) are clustered along the positive ends of the X and Y axes, whereas other correlations are scattered throughout the positive and negative regions.

Table 1. Linear measurements for the calcaneus.

Calcaneus	
1	Proximodistal tuber length
2	Proximodistal neck length
3	Minimum dorsoplantar tuber height
4	Dorsoplantar neck height
5	Minimum mediolateral tuber width
6	Mediolateral tuber width at the peroneal trochlea
7	Maximum length
8	Sustentaculum breadth
9	Calcaneal body
10	Overall articular dimension
11	Tuberosity breadth
12	Posterior talar articular surface a
13	Posterior talar articular surface b
14	Dorso/plantar cuboid facet dimension
15	Medio/lateral cuboid facet dimension
16	Talar facet articular surface area
17	Cuboid facet area
18	Geometric mean

Table 2. Linear measurements for the navicular.

Navicular	
1	Talar facet major axis (dorsoplantar) diameter
2	Talar facet minor axis (mediolateral) diameter
3	Ectocuneiform facet dorsoplantar diameter
4	Ectocuneiform facet mediolateral diameter
5	Mesocuneiform facet dorsoplantar diameter
6	Mesocuneiform facet mediolateral diameter
7	Entocuneiform facet mediolateral diameter
8	Entocuneiform facet dorsoplantar diameter
9	Navicular maximum length
10	Cuboid facet dorsoplantar diameter
11	Cuboid facet mediolateral diameter
16	Sustentaculum tali projection
17	Talar facet area
18	Ectocuneiform facet area
19	Mesocuneiform facet area
20	Entocuneiform facet area
21	Cuboid facet area
22	Geometric mean

Table 3. Linear measurements for the talus.

Talus	
1	Distance from the most distolateral point on the talar trochlea to the most medial point on the cotylar fossa
2	Medial body length
3	Lateral body height
4	Mid-trochlear width
5	Medial body height
6	Medial height (overall)
7	Distance from the most lateral point on fibular facet to the medial aspect of the cotylar fossa
8	Anteroposterior length of the ectal facet
9	Mediolateral width of the distal ectal facet
10	Head width
11	Head height
12	Talar length
13	Talar neck length
14	Talofibular lateral projection
15	Plantar facet length
16	Plantar facet width
17	Talar width
18	Lateral body height
19	Anterior trochlear width
20	Posterior trochlear width
21	Talar head area
22	Anteroposterior talar facet difference
23	Plantar facet area
24	Mediolateral talar body height difference
25	Geometric mean

Table 4. MANOVA results summary for the calcaneus, navicular, and talus.

MANOVA Summary		
Calcaneus	Wilk's lambda	0.00476
	F	29.24
	df1	36
	df2	78
	p-value	< 0.001
Navicular	Wilk's lambda	0.0156
	F	18.39
	df1	36
	df2	80
	p-value	< 0.001
Talus	Wilk's lambda	0.004319
	F	23.91
	df1	44
	df2	74
	p-value	< 0.001

Table 5. Summary of ANOVA results for the size-adjusted data of the calcaneus, navicular, and talus.

ANOVA Summary				
		F	df	p-value
Calcaneus	Cuboid facet area	1.24	2	< 0.001
	Talar articular surface area*	16.91	2,34	< 0.001
Navicular	Talar facet area	49.13	2	< 0.001
Talus	Talar head area	25.16	2	< 0.001
***Welch's test**				

Table 6. Bonferroni multiple comparisons of the calcaneus species means demonstrating which species means are significantly different from one another for talar articular surface area and cuboid facet area.

Multiple Comparisons						
Species		Mean Difference	Std. Error	Sig.	95% Confidence Interval	
					Lower Bound	Upper Bound
Homo	*Gorilla*	-3.36	1.23	0.025	-6.39	-0.33
	Pan	3.20	1.19	0.029	0.26	6.15
Gorilla	*Homo*	3.36	1.23	0.025	0.33	6.39
	Pan	6.56	1.26	< 0.01	3.47	9.66
Pan	*Homo*	-3.20	1.19	0.029	-6.15	-0.26
	Gorilla	-6.56	1.26	0.000	-9.66	-3.47

Table 7. Bonferroni-corrected p-values for multiple comparisons of the navicular data from the MANOVA.

Bonferroni-corrected p-values			
	Homo sapiens	***Gorilla gorilla***	***Pan troglodytes***
Homo sapiens		< 0.001	< 0.001
Gorilla gorilla	< 0.001		< 0.001
Pan troglodytes	< 0.001	< 0.001	

Table 8. Bonferroni multiple comparisons of the navicular species means demonstrating which species means are significantly different from one another for talar facet area.

Multiple Comparisons						
Species		Mean Difference	Std. Error	Sig.	95% Confidence Interval	
					Lower Bound	Upper Bound
Homo	*Gorilla*	-1.18	0.62	0.19	-2.71	0.36
	Pan	4.81	0.63	0.00	3.25	6.36
Gorilla	*Homo*	1.18	0.62	0.19	-0.36	2.71
	Pan	5.98	0.64	0.00	4.41	7.56
Pan	*Homo*	-4.81	0.63	0.00	-6.36	-3.25
	Gorilla	-5.98	0.64	0.00	-7.56	-4.41
***. The mean difference is significant at the 0.05 level.**						

Table 9. Bonferroni-corrected p-values for multiple comparisons of the talus data from the MANOVA.

Bonferroni-corrected p-values			
	Homo sapiens	***Gorilla gorilla***	***Pan troglodytes***
Homo sapiens		< 0.001	< 0.001
Gorilla gorilla	< 0.001		< 0.001
Pan troglodytes	< 0.001	< 0.001	

Table 10. Bonferroni multiple comparisons of the talus species means demonstrating which species means are significantly different from one another for talar head area.

Multiple Comparisons						
Species		Mean Difference	Std. Error	Sig.	95% Confidence Interval	
					Lower Bound	Upper Bound
Homo	*Gorilla*	4.22	0.88	0.00	2.05	6.40
	Pan	5.92	0.86	0.00	3.81	8.04
Gorilla	*Homo*	-4.22	0.88	0.00	-6.40	-2.05
	Pan	1.70	0.88	0.18	-0.47	3.87
Pan	*Homo*	-5.92	0.86	0.00	-8.04	-3.81
	Gorilla	-1.70	0.88	0.18	-3.87	0.47

Table 11. Values for the median correlation coefficients of articular and non-articular surfaces for each species, separated by bone. X = no correlation coefficients generated for non-articular surfaces.

Median Correlations				
		H. sapiens	*G. gorilla*	*P. troglodytes*
Calcaneus	Articular surface-articular surface	0.27	0.32	0.28
	Non-articular surface-non-articular surface	0.31	0.38	0.22
	Articular surface-non-articular surface	0.25	0.38	0.31
Navicular	Articular surface-articular surface	0.25	0.23	0.30
	Non-articular surface-non-articular surface	X	X	X
	Articular surface-non-articular surface	0.24	0.23	0.15
Talus	Articular surface-articular surface	0.16	0.25	0.31
	Non-articular surface-non-articular surface	-0.02	0.29	0.16
	Articular surface-non-articular surface	0.02	0.28	0.26

Supplemental Materials

Table S1. Principal components loadings for the first two axes of the scaled variance/covariance matrix for the calcaneus.

PC Loadings of the Calcaneus		
	PC 1	**PC 2**
1	0.017691	0.0097652
2	0.010674	-0.0050439
3	0.0078097	-0.0088003
4	0.005931	-0.0063416
5	0.0076168	-0.0010086
6	0.0055783	0.00036182
7	0.030928	0.0050202
8	0.0054967	0.00229
9	0.026782	0.0038184
10	0.016084	0.0006215
11	0.0095518	-0.0019601
12	0.010156	-0.0066727
13	0.0097313	-0.01009
14	0.0093683	0.0083128
15	0.0090558	0.010562
16	0.0075144	0.0069879
Talar Articular SA	0.74123	-0.67
Cuboid Facet Area	0.66895	0.74191

Table S2. Principal components loadings for the first five axes of the scaled variance/covariance matrix for the navicular.

PC Loadings of the Navicular					
	PC 1	PC 2	PC 3	PC 4	PC 5
1	0.011977	-0.017391	0.0015027	-0.0020918	0.00083972
2	0.0087512	0.0028814	-0.0093057	0.001005	-0.0016396
3	0.0056502	0.010791	0.0086361	0.0052752	-0.021378
4	0.0045521	-0.0033725	0.0049447	0.002878	-0.010102
5	0.0062114	0.0057022	0.0062098	-0.0083635	0.00011229
6	0.0072038	0.0040232	0.0091429	-0.019954	0.0062691
7	0.0071494	0.0040204	0.0041195	0.0081851	0.0057022
8	0.0082013	0.016785	-0.0040267	0.0096659	0.0079143
Navicular Maximum Length	0.0166	-0.0191	0.019302	0.0048311	-0.0051703
10	-0.0014711	-0.017355	0.028746	0.010186	0.0072896
11	0.0014833	-0.0057458	0.006615	0.0046172	0.0074957
Talar Facet Area	0.77542	-0.52733	-0.34507	-0.01513	-0.025273
Ectocuneiform Facet Area	0.26787	0.18096	0.37775	0.21815	-0.83915
Mesocuneiform Facet Area	0.35926	0.25915	0.43303	-0.76671	0.16623
Entocuneiform Facet Area	0.44383	0.61631	0.0030261	0.50627	0.40755
Cuboid Facet Area	0.012244	-0.4906	0.74102	0.32743	0.31721

Table S3. Principal components loadings for the first three axes of the scaled variance/covariance matrix for the talus.

PC Loadings of the Talus			
	PC 1	**PC 2**	**PC 3**
1	0.013287	-0.0040599	0.28869
2	0.01208	-0.0047194	0.30696
3	0.011793	0.002749	-0.018464
4	0.0081468	-0.0068592	0.17238
5	0.006491	-0.0022598	0.026214
6	0.0095374	0.0013168	0.051021
7	0.013275	-0.0056392	0.35707
8	0.012727	-0.0080985	0.19561
9	0.0073507	-0.0042042	0.12329
10	0.0084235	0.013861	-0.045654
11	0.0077757	0.0079672	0.059791
12	0.015634	-0.0032101	0.34331
13	0.00443	-0.001308	0.16397
14	0.0010611	-0.0057411	0.12491
15	0.013472	-0.0073019	0.12541
16	0.0094719	-0.0072074	-0.072201
17	0.010444	-0.010871	0.40015
18	0.010411	-0.0043582	0.15236
19	0.012887	-0.0070453	0.23515
20	0.010574	0.0010815	-0.036312
Talar Head Area	0.58233	0.81249	-0.0020099
AP Talar Facet Diff	0.0023133	-0.0081268	0.27146
Plantar Facet Area	0.81159	-0.58217	-0.040413

Table S4. PCA loadings based on the correlation matrices for the calcaneus of *H. sapiens*, G. *gorilla* and *P. troglodytes*.

	PC1	**PC2**	**PC3**	**PC4**	**PC5**	**PC6**
H. sapiens						
_1_GEOM	0.703	0.251	-0.279	0.087	-0.219	-0.347
_2_GEOM	0.529	-0.513	-0.402	0.055	0.001	-0.16
_3_GEOM	0.337	-0.626	0.224	-0.515	-0.15	0.155
_4_GEOM	-0.493	-0.449	-0.271	0.402	0.251	-0.156
_5_GEOM	0.339	-0.31	-0.51	0.623	0.123	0.044
_6_GEOM	-0.896	0.023	0.089	0.373	0.019	-0.013
_7_GEOM	0.72	-0.111	0.094	0.063	-0.4	-0.342
_8_GEOM	0.408	0.355	0.234	-0.041	0.341	-0.577
_9_GEOM	0.842	0.002	0.177	0.142	0.135	-0.241
_10_GEOM	0.844	0.095	-0.072	-0.11	0.28	0.317
_11_GEOM	0.298	-0.375	-0.412	0.232	-0.539	0.384
_12_GEOM	0.629	-0.418	-0.187	0.047	0.493	0.111
_13_GEOM	0.25	-0.636	0.675	0.043	0	0.118
_14_GEOM	0.474	0.404	-0.433	-0.351	0.296	0.363
_15_GEOM	0.537	0.313	0.286	0.597	-0.277	0.104
_16_GEOM	0.456	0.363	0.688	0.08	-0.133	0.246
CFA	0.108	0.759	0.013	0.42	0.159	0.315
TASA	0.015	-0.513	0.628	0.348	0.354	0.115
G. gorilla						
_1_GEOM	-0.298	0.659	0.293	-0.326	-0.114	0.341
_2_GEOM	0.757	-0.355	0.261	-0.158	-0.135	0.053
_3_GEOM	0.43	-0.365	-0.496	-0.413	0.052	0.329
_4_GEOM	-0.265	-0.051	0.447	0.288	0.625	0.262
_5_GEOM	0.88	0.008	-0.079	-0.207	0.18	0.051
_6_GEOM	-0.893	0.142	0.014	-0.199	0.25	-0.19
_7_GEOM	0.72	0.621	0.113	0.127	-0.129	0.153
_8_GEOM	0.234	-0.677	0.265	0.213	-0.348	0.419
_9_GEOM	0.631	0.569	0.228	0.141	-0.184	0.363
_10_GEOM	0.726	-0.16	0.339	0.209	-0.133	-0.159
_11_GEOM	0.606	0.024	0.382	0.03	-0.327	-0.51
_12_GEOM	0.462	-0.256	0.421	0.255	0.33	0.025
_13_GEOM	0.781	-0.248	-0.1	-0.023	0.366	-0.003
_14_GEOM	0.682	0.35	-0.443	0.29	0.206	0.156
_15_GEOM	-0.395	-0.355	-0.492	0.521	-0.216	0.153
_16_GEOM	-0.651	0.144	0.189	0.664	0.016	-0.027
CFA	0.501	0.306	-0.65	0.378	-0.047	-0.168
TASA	0.885	0.062	-0.024	0.035	0.259	-0.257

Table S4. Continued from previous page.

	PC1	**PC2**	**PC3**	**PC4**	**PC5**	**PC6**
P. troglodytes						
_1_GEOM	0.782	-0.22	-0.231	-0.252	-0.12	0
_2_GEOM	0.351	-0.343	0.498	0.568	0.075	0.065
_3_GEOM	-0.546	-0.429	0.34	0.001	-0.046	0.22
_4_GEOM	-0.167	0.819	-0.147	0.081	-0.24	-0.064
_5_GEOM	0.137	-0.535	0.388	-0.188	0.561	0.061
_6_GEOM	-0.841	0.299	0.086	-0.165	0.159	0.105
_7_GEOM	0.82	-0.354	-0.198	0.051	0.054	-0.01
_8_GEOM	0.423	-0.148	-0.512	0.499	-0.191	0.026
_9_GEOM	0.911	-0.065	0.102	0.031	0.124	-0.141
_10_GEOM	0.613	-0.077	0.202	0.481	-0.31	-0.218
_11_GEOM	0.482	0.321	0.267	-0.342	-0.251	-0.328
_12_GEOM	0.337	0.085	0.694	0.02	-0.409	0.338
_13_GEOM	0.183	0.644	0.117	0.463	0.509	-0.041
_14_GEOM	0.757	0.117	-0.193	-0.119	0.406	-0.156
_15_GEOM	0.734	0.07	-0.046	-0.258	-0.123	0.533
_16_GEOM	0.391	0.158	0.526	-0.405	-0.041	-0.431
CFA	0.768	0.278	-0.218	-0.302	0.1	0.367
TASA	0.351	0.751	0.304	0.19	0.175	0.26

Table S5. Factor loadings based on the correlation matrices for the calcaneus of *H. sapiens*, G. *gorilla* and *P. troglodytes*.

	Factor 1	**Factor 2**	**Factor 3**	**Factor 4**	**Factor 5**	**Factor 6**
H. sapiens						
_1_GEOM	0.249	-0.08	-0.316	0.119	0.792	-0.029
_2_GEOM	0.317	-0.506	0.05	-0.352	0.454	0.213
_3_GEOM	0.302	0.236	0.423	-0.671	0.147	0.265
_4_GEOM	-0.369	-0.701	0.089	-0.111	-0.344	0.004
_5_GEOM	0.189	-0.799	0.04	0.211	0.252	0.305
_6_GEOM	-0.721	-0.164	0.008	0.213	-0.597	-0.036
_7_GEOM	0.082	0.058	0.115	-0.098	0.882	0.097
_8_GEOM	0.149	0.052	-0.007	0.114	0.457	-0.742
_9_GEOM	0.417	-0.077	0.281	0.119	0.716	-0.226
_10_GEOM	0.878	0.027	0.118	0.155	0.327	0.027
_11_GEOM	0.109	-0.224	-0.026	-0.039	0.268	0.869
_12_GEOM	0.691	-0.473	0.32	-0.144	0.194	-0.025
_13_GEOM	0.013	0.107	0.913	-0.246	0.147	0.101
_14_GEOM	0.843	0.092	-0.424	0.134	-0.023	-0.005
_15_GEOM	0.023	0.096	0.245	0.694	0.574	0.175
_16_GEOM	0.183	0.603	0.423	0.469	0.315	-0.044
CFA	0.186	0.106	-0.184	0.893	-0.063	-0.086
TASA	-0.059	-0.176	0.923	0.045	-0.122	-0.117
G. gorilla						
_1_GEOM	-0.227	0.792	-0.245	-0.161	-0.069	-0.274
_2_GEOM	0.393	0.067	0.023	0.536	0.069	0.602
_3_GEOM	0.238	-0.14	0.163	0.826	-0.147	-0.198
_4_GEOM	-0.017	0.037	-0.16	-0.233	0.838	-0.176
_5_GEOM	0.021	0.155	0.416	0.694	0.111	0.41
_6_GEOM	-0.533	-0.135	-0.505	-0.381	0.026	-0.502
_7_GEOM	0.013	0.668	0.598	0.106	-0.011	0.399
_8_GEOM	0.908	-0.111	-0.178	0.117	0.113	0.176
_9_GEOM	0.19	0.771	0.48	0.065	0.055	0.301
_10_GEOM	0.297	0.043	0.221	0.152	0.132	0.758
_11_GEOM	0.01	0.079	0.067	0.022	-0.174	0.916
_12_GEOM	0.211	-0.048	0.093	0.132	0.593	0.455
_13_GEOM	0.078	-0.153	0.401	0.627	0.316	0.366
_14_GEOM	-0.014	0.149	0.909	0.274	0.084	0.055
_15_GEOM	0.43	-0.514	0.194	-0.359	-0.18	-0.466
_16_GEOM	0.033	-0.099	-0.033	-0.894	0.228	-0.241
CFA	-0.085	-0.121	0.914	0.052	-0.271	0.083
TASA	-0.133	-0.003	0.531	0.457	0.185	0.616

Table S5. Continued from previous page.

	Factor 1	**Factor 2**	**Factor 3**	**Factor 4**	**Factor 5**	**Factor 6**
P. troglodytes						
_1_GEOM	0.734	-0.238	0.213	0.372	0.074	-0.073
_2_GEOM	-0.127	0.225	-0.052	0.627	0.465	0.378
_3_GEOM	-0.467	-0.308	-0.234	-0.237	0.347	0.323
_4_GEOM	-0.091	0.379	0.098	-0.201	-0.767	0.004
_5_GEOM	0.069	-0.009	0.087	-0.059	0.891	0.005
_6_GEOM	-0.514	0.104	-0.155	-0.744	-0.122	-0.008
_7_GEOM	0.633	-0.092	0.051	0.592	0.26	-0.119
_8_GEOM	0.284	-0.038	-0.379	0.662	-0.234	-0.175
_9_GEOM	0.575	0.202	0.371	0.559	0.243	-0.017
_10_GEOM	0.079	0.109	0.212	0.827	-0.056	0.217
_11_GEOM	0.267	0.047	0.746	0.107	-0.197	0.116
_12_GEOM	0.113	0.074	0.287	0.168	0.034	0.868
_13_GEOM	-0.02	0.955	0.003	0.093	-0.07	-0.112
_14_GEOM	0.649	0.324	0.27	0.256	0.177	-0.362
_15_GEOM	0.874	0.022	0.028	0.091	-0.002	0.371
_16_GEOM	0.096	0.065	0.872	0.036	0.134	0.11
CFA	0.94	0.219	0.1	0.014	-0.072	0.065
TASA	0.251	0.818	0.154	-0.033	-0.207	0.336

Table S6. PCA loadings based on the correlation matrices for the navicular of *H. sapiens*, G. *gorilla* and *P. troglodytes*.

	PC1	**PC2**	**PC3**	**PC4**	**PC5**
H. sapiens					
_1_GEOM	0.346	-0.197	-0.117	0.738	-0.397
_2_GEOM	-0.698	0.295	0.376	0.024	0.473
_3_GEOM	0.706	-0.163	-0.145	-0.448	0.323
_4_GEOM	0.477	-0.384	0.452	0.003	-0.193
_5_GEOM	0.811	0.209	-0.048	-0.163	0.057
_6_GEOM	0.62	0.251	0.655	0.026	-0.121
_7_GEOM	0.418	0.121	0.572	0.248	0.314
_8_GEOM	0.569	-0.286	-0.589	0.224	0.347
_10_GEOM	0.347	0.765	-0.021	-0.031	-0.293
_11_GEOM	0.461	0.437	-0.286	0.339	0.415
CFA_GEOM	0.394	0.764	-0.156	0.284	0.013
ECFA_GEOM	0.465	-0.649	0.2	-0.338	0.124
ENTFA_GEOM	0.436	-0.475	0.079	0.462	0.482
MSFA_GEOM	0.653	0.077	0.632	-0.001	-0.126
NAVICULAR MAXIMUM LENGTH_GEOM	0.694	-0.294	-0.386	-0.036	-0.468
TFA_GEOM	-0.596	-0.426	0.257	0.526	-0.128
G. gorilla					
_1_GEOM	-0.203	0.171	0.098	-0.237	0.819
_2_GEOM	-0.904	-0.215	0.065	-0.19	-0.02
_3_GEOM	0.138	0.508	0.462	-0.153	-0.393
_4_GEOM	0.073	0.344	0.306	-0.301	0.274
_5_GEOM	-0.24	0.432	0.705	0.163	0.226
_6_GEOM	-0.06	-0.47	0.593	0.318	0.418
_7_GEOM	-0.099	0.292	0.525	-0.443	0.033
_8_GEOM	0.126	-0.182	0.276	0.815	-0.078
_10_GEOM	0.026	0.808	-0.236	0.276	0.3
_11_GEOM	-0.707	0.323	-0.091	0.386	0.018
CFA_GEOM	0.035	0.706	-0.485	0.359	0.239
ECFA_GEOM	0.69	0.424	0.199	-0.331	-0.243
ENTFA_GEOM	0.79	-0.133	0.07	0.061	-0.066
MSFA_GEOM	0.662	-0.332	0.327	0.214	0.38
NAVICULAR MAXIMUM LENGTH_GEOM	0.899	0.224	-0.059	0.196	0.021
TFA_GEOM	0.39	-0.293	-0.472	-0.384	0.564

Table S6. Continued from previous page.

	PC1	PC2	PC3	PC4	PC5
P. troglodytes					
_1_GEOM	0.685	0.314	0.14	-0.144	0.505
_2_GEOM	-0.4	0.855	0.003	-0.053	-0.204
_3_GEOM	0.446	0.614	-0.265	-0.106	-0.231
_4_GEOM	0.09	0.642	-0.406	-0.52	0.223
_5_GEOM	0.188	-0.114	0.791	-0.203	-0.209
_6_GEOM	0.238	0.628	0.478	0.227	-0.118
_7_GEOM	0.008	-0.001	-0.36	0.699	0.271
_8_GEOM	0.184	0.58	-0.104	0.588	-0.243
_10_GEOM	0.844	0.184	0.168	0.241	0.028
_11_GEOM	0.918	0.158	-0.179	-0.138	-0.049
CFA_GEOM	0.863	0.107	0.171	0.16	0.121
ECFA_GEOM	-0.401	0.61	-0.166	-0.306	0.212
ENTFA_GEOM	-0.347	0.194	-0.106	0.878	0.158
MSFA_GEOM	-0.239	0.199	0.921	0.12	-0.046
NAVICULAR MAXIMUM LENGTH_GEOM	0.398	-0.853	0.011	0.062	0.2
TFA_GEOM	-0.408	0.327	0.473	-0.033	0.658

Table S7. Factor loadings based on the correlation matrices for the navicular of *H. sapiens*, G. *gorilla* and *P. troglodytes*.

	Factor 1	**Factor 2**	**Factor 3**	**Factor 4**	**Factor 5**
H. sapiens					
_1_GEOM	0.638	0.193	0.179	0.343	-0.529
_2_GEOM	-0.932	-0.005	-0.088	-0.084	-0.238
_3_GEOM	0.234	-0.096	0.19	0.295	0.814
_4_GEOM	0.323	-0.324	0.633	0.071	0.027
_5_GEOM	0.336	0.336	0.388	0.167	0.574
_6_GEOM	0.068	0.227	0.902	-0.069	0.13
_7_GEOM	-0.225	0.143	0.704	0.331	0.022
_8_GEOM	0.44	0.089	-0.201	0.759	0.326
_10_GEOM	0.137	0.761	0.221	-0.34	0.175
_11_GEOM	-0.008	0.663	0.027	0.531	0.223
CFA_GEOM	0.053	0.899	0.139	0.078	0.095
ECFA_GEOM	0.261	-0.623	0.352	0.23	0.418
ENTFA_GEOM	0.093	-0.195	0.285	0.859	-0.032
MSFA_GEOM	0.152	0.078	0.892	-0.014	0.152
NAVICULAR MAXIMUM LENGTH_GEOM	0.929	0.003	0.076	0.081	0.25
TFA_GEOM	-0.149	-0.402	-0.07	0.085	-0.837
G. gorilla					
_1_GEOM	-0.219	0.256	-0.038	0.37	0.754
_2_GEOM	-0.909	-0.233	0.122	-0.009	0.02
_3_GEOM	0.088	0.004	-0.96	-0.05	-0.088
_4_GEOM	0.11	0.138	0.051	0.01	0.089
_5_GEOM	-0.233	0.245	-0.517	0.552	-0.061
_6_GEOM	-0.057	-0.281	0.071	0.883	0.03
_7_GEOM	-0.082	-0.113	-0.185	-0.024	-0.011
_8_GEOM	0.177	0.11	0.177	0.56	-0.638
_10_GEOM	0.063	0.916	-0.112	-0.054	0.063
_11_GEOM	-0.674	0.489	0.03	0.073	-0.253
CFA_GEOM	0.075	0.938	0.056	-0.172	0.027
ECFA_GEOM	0.656	-0.012	-0.604	-0.261	0.08
ENTFA_GEOM	0.823	-0.133	0.262	-0.011	-0.226
MSFA_GEOM	0.658	-0.18	0.051	0.602	0.158
NAVICULAR MAXIMUM LENGTH_GEOM	0.906	0.241	-0.122	0.012	-0.028
TFA_GEOM	0.362	-0.078	0.38	-0.1	0.79

Table S7. Continued from previous page.

	Factor 1	**Factor 2**	**Factor 3**	**Factor 4**	**Factor 5**
P. troglodytes					
_1_GEOM	0.836	0.041	-0.045	-0.117	0.383
_2_GEOM	-0.155	0.93	0.177	0.119	0.034
_3_GEOM	0.533	0.559	-0.142	-0.028	-0.307
_4_GEOM	0.276	0.695	-0.472	-0.28	0.211
_5_GEOM	0.139	-0.188	0.728	-0.416	0.009
_6_GEOM	0.427	0.423	0.589	0.19	0.023
_7_GEOM	0.069	-0.141	-0.272	0.769	0.043
_8_GEOM	0.316	0.427	0.159	0.623	-0.302
_10_GEOM	0.865	-0.115	0.18	0.132	-0.148
_11_GEOM	0.873	-0.013	-0.201	-0.185	-0.29
CFA_GEOM	0.875	-0.191	0.127	0.052	-0.067
ECFA_GEOM	-0.167	0.707	-0.185	-0.072	0.362
ENTFA_GEOM	-0.201	0.07	0.072	0.95	0.107
MSFA_GEOM	-0.108	0.087	0.924	-0.005	0.299
NAVICULAR MAXIMUM LENGTH_GEOM	0.154	-0.931	-0.161	-0.113	-0.034
TFA_GEOM	-0.118	0.218	0.291	0.079	0.882

Table S8. PCA loadings based on the correlation matrices for the talus of *H. sapiens*, G. *gorilla* and *P. troglodytes*.

	PC1	PC2	PC3	PC4	PC5	PC6	PC7
H. sapiens							
_1_GEOM	0.692	0.389	0.441	0.094	-0.05	-0.051	-0.103
_2_GEOM	0.591	-0.282	0.222	-0.604	0.229	0.239	0.035
_3_GEOM	0.759	0.257	0.457	0.145	-0.282	-0.043	0.05
_4_GEOM	0.236	0.072	-0.05	0.104	0.754	0.067	-0.367
_5_GEOM	-0.212	-0.161	-0.731	0.1	-0.266	0.025	-0.155
_6_GEOM	0.117	-0.229	0.188	-0.34	-0.481	0.59	-0.381
_7_GEOM	0.014	0.619	0.597	-0.076	0.257	0.048	-0.167
_8_GEOM	0.659	0.503	-0.307	-0.363	0.069	-0.044	0.088
_9_GEOM	0.435	-0.538	-0.321	-0.244	-0.101	-0.44	0.028
_10_GEOM	0.419	-0.664	0.508	0.011	0.061	0.066	0.283
_11_GEOM	-0.12	-0.591	0.558	0.285	0.118	-0.242	-0.277
_12_GEOM	-0.293	0.398	0.497	-0.264	-0.255	-0.184	0.255
_13_GEOM	-0.324	0.026	0.465	0.281	0.012	0.548	0.294
_14_GEOM	0.274	0.696	0.266	-0.265	0.174	-0.294	0.109
_15_GEOM	0.431	0.695	-0.367	-0.03	-0.016	0.225	0.274
_16_GEOM	0.664	-0.315	-0.292	0.51	0.202	0.012	0.094
_17_GEOM	-0.395	0.533	0.029	0.379	0.226	0.377	-0.055
_18_GEOM	0.433	-0.593	-0.082	0.144	0.282	0.082	0.097
_19_GEOM	0.78	0.298	0.155	0.105	-0.091	-0.06	-0.445
_20_GEOM	0.734	-0.185	-0.159	0.061	-0.399	0.249	-0.136
MLTALARBHDIFF	-0.082	-0.376	-0.253	-0.712	0.402	0.289	0.032
PFA_GEOM	0.654	0.268	-0.514	0.34	0.058	0.156	0.242
THA_GEOM	0.325	-0.653	0.531	0.109	-0.003	0.031	0.237
G. gorilla							
_1_GEOM	0.357	0.45	0.012	-0.622	-0.096	0.248	0.149
_2_GEOM	0.003	-0.085	0.798	0.25	0.344	0.343	-0.003
_3_GEOM	0.88	0.208	0.121	-0.259	0.131	-0.035	-0.051
_4_GEOM	0.303	0.216	-0.369	0.11	0.187	-0.193	0.644
_5_GEOM	0.441	-0.66	0.029	-0.069	0.205	0.476	0.198
_6_GEOM	0.275	0.418	-0.539	0.287	0.18	0.453	0.036
_7_GEOM	-0.358	0.502	0.628	-0.128	-0.113	0.067	-0.15
_8_GEOM	0.106	0.592	0.565	0.001	0.242	-0.226	0.317
_9_GEOM	0.417	0.371	0.32	0.395	-0.304	-0.287	-0.015
_10_GEOM	0.494	0.328	0.125	0.166	-0.49	0.456	-0.174
_11_GEOM	0.594	0.561	-0.232	0.116	0.377	0.022	-0.159
_12_GEOM	0.502	0.306	0.555	0.257	0.288	-0.309	0.035

Table S8. Continued from previous page.

	PC1	PC2	PC3	PC4	PC5	PC6	PC7
G. gorilla							
_13_GEOM	0.577	0.164	-0.232	0.564	0.1	-0.259	-0.269
_14_GEOM	0.062	-0.378	0.616	0.267	-0.35	-0.318	0.052
_15_GEOM	-0.592	0.535	0.43	-0.3	0.129	-0.019	0.111
_16_GEOM	0.186	-0.066	-0.218	0.527	-0.48	0.209	0.514
_17_GEOM	-0.218	0.778	-0.414	-0.168	0.106	-0.059	0.143
_18_GEOM	-0.588	0.26	-0.567	-0.019	-0.324	-0.278	-0.126
_19_GEOM	0.659	-0.317	0.385	-0.353	-0.24	0.064	0.136
_20_GEOM	0.659	0.132	0.231	-0.403	-0.43	-0.153	-0.005
MLTALARBHDIFF	-0.649	-0.091	0.544	0.322	0.161	0.277	0.011
PFA_GEOM	-0.659	0.489	0.195	0.137	-0.267	0.137	0.308
THA_GEOM	0.059	0.793	0.067	0.161	-0.212	0.37	-0.25
P. troglodytes							
_1_GEOM	0.536	0.166	0.274	0.03	-0.284	0.429	0.385
_2_GEOM	0.158	0.697	-0.276	0.37	0.128	-0.392	0.092
_3_GEOM	0.741	0.253	-0.142	0.169	0.451	-0.18	0.131
_4_GEOM	-0.143	-0.203	0.357	0.472	0.048	-0.189	-0.371
_5_GEOM	-0.256	-0.555	-0.603	0.155	0.251	0.091	-0.249
_6_GEOM	-0.353	0.485	-0.365	0.077	0.402	0.223	0.171
_7_GEOM	0.655	0.236	0.495	-0.219	0.12	0.152	0.166
_8_GEOM	0.582	0.525	0.183	-0.16	-0.051	-0.394	-0.248
_9_GEOM	-0.509	0.651	0.115	0.111	-0.228	0.061	0.067
_10_GEOM	0.683	-0.302	0.077	0.348	0.099	-0.027	0.307
_11_GEOM	0.668	0.217	-0.167	0.338	-0.241	0.117	-0.21
_12_GEOM	0.165	0.086	-0.035	-0.14	-0.788	-0.499	0.123
_13_GEOM	-0.483	0.034	0.569	0.44	-0.223	0.21	0.172
_14_GEOM	0.311	0.299	0.507	0.178	0.43	-0.415	-0.056
_15_GEOM	0.678	0.351	-0.31	-0.417	-0.002	0.182	-0.073
_16_GEOM	-0.352	0.8	0.009	0.221	0.077	0.16	-0.257
_17_GEOM	0.04	0.186	0.464	-0.396	-0.162	0.216	-0.53
_18_GEOM	-0.468	0.542	0.482	0.125	0.21	0.191	0.128
_19_GEOM	0.295	-0.12	-0.089	0.765	-0.258	0.277	-0.258
_20_GEOM	0.756	-0.194	0.255	0.1	0.054	0.081	-0.231
MLTALARBHDIFF	-0.42	0.557	-0.418	0.201	-0.363	-0.196	0.057
PFA_GEOM	0.284	0.741	-0.389	-0.179	0.002	0.327	-0.155
THA_GEOM	0.835	-0.058	-0.277	0.254	-0.189	0.18	0.077

Table S9. Factor loadings based on the correlation matrices for the talus of *H. sapiens*, G. *gorilla* and *P. troglodytes*.

	Factor 1	**Factor 2**	**Factor 3**	**Factor 4**	**Factor 5**	**Factor 6**	**Factor 7**
H. sapiens							
_1_GEOM	0.202	-0.111	0.854	0.215	0.027	-0.018	0.14
_2_GEOM	0.247	-0.076	0.058	0.687	0.425	0.312	0.365
_3_GEOM	0.193	-0.025	0.885	0.333	0.071	0.022	-0.137
_4_GEOM	0.012	0.211	0.094	0.004	-0.137	-0.07	0.839
_5_GEOM	0.052	0.444	-0.366	-0.521	0.12	0.21	-0.218
_6_GEOM	-0.093	-0.019	0.072	0.092	0.951	-0.04	-0.109
_7_GEOM	0.053	-0.591	0.439	-0.004	-0.048	-0.389	0.378
_8_GEOM	0.811	-0.048	0.329	-0.014	0.026	0.334	0.217
_9_GEOM	-0.013	0.303	-0.043	0.236	-0.015	0.831	-0.078
_10_GEOM	-0.287	0.176	0.133	0.901	0.079	0.095	-0.07
_11_GEOM	-0.882	0.049	0.119	0.305	-0.074	0.021	0.101
_12_GEOM	0.014	-0.764	0.108	0.033	-0.094	-0.145	-0.313
_13_GEOM	-0.136	-0.093	-0.09	0.281	0.072	-0.799	-0.177
_14_GEOM	0.43	-0.569	0.439	0.004	-0.275	0.058	0.221
_15_GEOM	0.9	0.066	0.263	-0.164	-0.058	-0.132	0.004
_16_GEOM	0.119	0.832	0.277	0.275	-0.216	0.128	0.114
_17_GEOM	0.092	-0.06	-0.024	-0.38	-0.132	-0.76	0.17
_18_GEOM	-0.087	0.565	-0.041	0.514	-0.017	0.187	0.186
_19_GEOM	0.159	0.134	0.864	-0.038	0.2	0.191	0.272
_20_GEOM	0.23	0.509	0.445	0.166	0.468	0.247	-0.157
MLTALARBHDIFF	0.192	-0.066	-0.693	0.297	0.347	0.259	0.41
PFA_GEOM	0.679	0.613	0.309	-0.019	-0.179	-0.008	0.01
THA_GEOM	-0.389	0.175	0.154	0.81	0.052	0.044	-0.134
G. gorilla							
_1_GEOM	-0.116	0.278	0.384	0.746	0.118	0.023	-0.029
_2_GEOM	0.2	0.336	-0.192	-0.222	0.135	0.816	-0.138
_3_GEOM	0.45	-0.209	0.243	0.727	0.056	0.264	-0.117
_4_GEOM	0.266	-0.058	0.409	0.163	-0.43	-0.088	0.559
_5_GEOM	-0.298	-0.496	0	0.182	-0.109	0.735	0.153
_6_GEOM	0.087	-0.198	0.799	-0.09	0.3	0.006	0.28
_7_GEOM	0.091	0.79	-0.158	-0.004	0.309	0.018	-0.277
_8_GEOM	0.576	0.68	0.077	0.19	-0.151	0.177	0.034
_9_GEOM	0.707	0.09	-0.204	0.181	0.327	-0.078	0.224
_10_GEOM	0.153	-0.041	0.087	0.348	0.809	0.124	0.223
_11_GEOM	0.572	-0.153	0.692	0.213	0.137	0.026	-0.097
_12_GEOM	0.847	0.173	-0.053	0.176	-0.044	0.336	-0.06

Table S9. Continued from previous page.

	Factor 1	Factor 2	Factor 3	Factor 4	Factor 5	Factor 6	Factor 7
G. gorilla							
_13_GEOM	0.723	-0.513	0.196	-0.074	0.194	-0.095	0.069
_14_GEOM	0.265	0.022	-0.836	-0.004	0.034	0.187	0.131
_15_GEOM	-0.07	0.925	0.047	-0.076	-0.085	-0.084	-0.241
_16_GEOM	0.01	-0.185	-0.056	-0.062	0.235	-0.005	0.897
_17_GEOM	0.05	0.419	0.655	0.034	-0.051	-0.523	0.052
_18_GEOM	-0.249	0.095	0.084	-0.287	0.018	-0.879	0.021
_19_GEOM	0.023	-0.191	-0.342	0.739	0.034	0.428	0.063
_20_GEOM	0.217	-0.049	-0.202	0.865	0.192	-0.03	0.01
MLTALARBHDIFF	-0.146	0.505	-0.276	-0.649	0.095	0.381	-0.065
PFA_GEOM	-0.148	0.787	-0.018	-0.307	0.18	-0.232	0.306
THA_GEOM	0.221	0.389	0.402	0.045	0.726	-0.128	0.005
P. troglodytes							
_1_GEOM	0.139	-0.072	-0.044	0.333	-0.048	0.815	-0.011
_2_GEOM	0.209	0.57	0.562	0.201	-0.143	-0.09	-0.384
_3_GEOM	0.425	-0.149	0.67	0.309	0.179	0.138	-0.341
_4_GEOM	-0.619	-0.057	0.228	0.217	0.055	-0.259	0.177
_5_GEOM	0.025	-0.239	-0.403	0.114	0.319	-0.714	-0.223
_6_GEOM	0.232	0.607	-0.047	-0.168	0.441	-0.092	-0.29
_7_GEOM	0.226	-0.227	0.44	0.066	0.088	0.7	0.209
_8_GEOM	0.356	0.073	0.718	0.143	-0.345	0.15	0.288
_9_GEOM	-0.173	0.818	-0.059	-0.157	-0.116	0.14	0.09
_10_GEOM	-0.022	-0.517	0.264	0.445	0.04	0.311	-0.395
_11_GEOM	0.281	0.013	0.205	0.77	-0.141	0.128	0.034
_12_GEOM	0.058	0.003	-0.008	0.04	-0.963	0.096	-0.011
_13_GEOM	-0.791	0.325	-0.183	0	0.055	0.323	0.057
_14_GEOM	-0.181	-0.013	0.876	-0.035	0.102	0.147	0.042
_15_GEOM	0.861	-0.061	0.158	0.213	-0.037	0.229	0.147
_16_GEOM	-0.005	0.89	0.164	0.061	0.197	-0.044	0.216
_17_GEOM	0.04	0.032	0.058	-0.057	-0.011	0.159	0.853
_18_GEOM	-0.359	0.626	0.153	-0.297	0.319	0.324	0.137
_19_GEOM	-0.258	0.017	-0.086	0.907	0.052	-0.046	-0.05
_20_GEOM	0.095	-0.517	0.348	0.496	0.068	0.224	0.223
MLTALARBHDIFF	0.061	0.78	-0.131	0.017	-0.382	-0.227	-0.22
PFA_GEOM	0.74	0.528	0.077	0.242	0.102	0.133	0.158
THA_GEOM	0.392	-0.302	0.072	0.738	-0.103	0.25	-0.219

Table S10. Factor analysis loadings for the first four axes of the scaled correlation matrix for the calcaneus.

Component Loadings				
	1	**2**	**3**	**4**
1/GEOM	0.679	0.416	-0.308	-0.007
2/GEOM	0.539	-0.359	0.488	0.284
3/GEOM	-0.598	0.275	0.549	-0.078
4/GEOM	-0.624	0.295	0.238	0.002
5/GEOM	0.127	-0.367	0.538	0.035
6/GEOM	-0.639	0.426	-0.440	0.173
7/GEOM	0.787	0.524	0.016	0.144
8/GEOM	0.542	-0.645	-0.265	0.002
9/GEOM	0.772	0.555	0.072	0.034
10/GEOM	0.717	-0.054	0.395	-0.187
11/GEOM	-0.009	-0.114	0.604	-0.231
12/GEOM	-0.109	0.288	0.742	-0.269
13/GEOM	0.449	-0.449	0.117	0.270
14/GEOM	0.592	-0.481	0.028	-0.093
15/GEOM	0.121	0.141	-0.056	-0.822
16/GEOM	0.469	-0.092	-0.460	-0.433
TALAR ARTICULAR SA	0.457	0.656	0.285	0.319
CUBOID FACET AREA	0.549	0.672	-0.047	-0.064

Table S11. Factor analysis loadings for the first four axes of the scaled correlation matrix for the navicular.

Component Loadings					
	1	**2**	**3**	**4**	**5**
1/GEOM	-0.377	-0.345	0.513	0.205	0.043
2/GEOM	0.401	0.668	-0.476	0.261	-0.097
3/GEOM	0.194	0.716	0.197	-0.510	0.174
4/GEOM	-0.594	0.428	0.090	-0.205	-0.268
5/GEOM	0.192	0.683	0.312	0.129	0.366
6/GEOM	0.149	0.406	0.636	0.462	-0.104
7/GEOM	-0.134	0.397	0.278	0.005	-0.776
8/GEOM	0.591	0.540	-0.028	0.009	0.224
NAVICULAR MAXIMUM LENGTH/GEOM	-0.379	-0.680	0.476	-0.267	0.099
10/GEOM	-0.864	0.317	0.131	-0.018	0.009
11/GEOM	-0.701	0.460	0.031	0.165	0.202
TFA/GEOM	0.641	-0.612	0.102	0.133	-0.025
ECFA/GEOM	0.506	0.139	0.324	-0.718	-0.019
MSFA/GEOM	0.698	-0.005	0.594	0.258	0.097
ENTFA/GEOM	0.841	0.056	0.163	-0.052	-0.204
CFA/GEOM	-0.851	0.146	0.196	0.009	0.132

Table S12. Factor analysis loadings for the first four axes of the scaled correlation matrix for the talus.

Component Loadings							
	1	**2**	**3**	**4**	**5**	**6**	**7**
1/GEOM	-0.240	0.684	0.182	0.088	0.320	0.108	0.004
2/GEOM	-0.377	0.237	0.423	0.275	-0.558	-0.299	0.183
3/GEOM	0.834	0.271	0.315	-0.088	0.091	0.098	0.060
4/GEOM	-0.285	-0.084	0.114	0.296	0.122	0.600	0.324
5/GEOM	0.552	-0.485	-0.057	-0.403	-0.376	0.173	0.080
6/GEOM	0.604	-0.148	-0.020	0.110	-0.031	-0.167	-0.140
7/GEOM	-0.657	0.484	0.198	0.016	0.280	-0.133	0.213
8/GEOM	0.015	0.743	0.215	0.104	-0.152	0.142	0.173
9/GEOM	-0.051	-0.031	0.215	0.617	-0.423	0.128	-0.388
10/GEOM	0.714	-0.159	0.346	0.322	0.084	-0.262	0.129
11/GEOM	0.464	-0.318	0.480	0.151	0.317	-0.181	0.173
12/GEOM	-0.249	0.412	0.534	-0.260	0.061	-0.071	-0.462
13/GEOM	-0.356	-0.328	0.304	0.283	0.278	0.221	-0.497
14/GEOM	-0.507	-0.396	0.427	0.085	-0.168	0.099	0.326
15/GEOM	0.106	0.926	-0.271	-0.098	-0.005	-0.033	-0.012
16/GEOM	0.658	0.044	-0.154	0.461	-0.171	0.279	-0.006
17/GEOM	-0.777	-0.093	-0.040	0.068	0.328	0.075	0.080
18/GEOM	-0.003	-0.049	-0.526	0.746	0.218	-0.075	0.046
19/GEOM	0.061	0.637	0.241	-0.103	-0.156	0.381	-0.012
20/GEOM	0.843	0.175	0.177	-0.010	0.004	0.209	0.054
THA/GEOM	0.704	0.398	0.147	0.201	0.212	-0.359	0.045
PLANTAR FACET AREA	0.284	0.834	-0.375	0.083	-0.063	0.051	-0.043

References

Ackermann, R. R. 2002. Patterns of covariation in the hominoid craniofacial skeleton: implications for paleoanthropological models. *Journal of Human Evolution* 42: 167-187.

Ackermann, R. R. 2005. Ontogenetic integration of the hominoid face. *Journal of Human Evolution* 48: 175-197.

Ackermann, R. R. 2009. Morphological integration and the interpretation of fossil hominin diversity. *Evolutionary Biology* 36: 149-156.

Ackermann, R. R. and Cheverud, J. M. 2000. Phenotypic covariance structure in tamarins (Genus *Saguinus*): A comparison of variation patterns using matrix correlation and common principal component analysis. *American Journal of Physical Anthropology* 111: 489-501.

Aiello, L. and Dean, C. 1990. An introduction to human evolutionary anatomy. London: Academic Press.

Berger, L. R., de Ruiter, D. J., Churchill, S. E., Schmid, P., Carlson, K. J., Dirks, P. H. G. M., and Kibii, J. M. 2010. *Australopithecus sediba*: A new species of Homo-like australopith from South Africa. Science 328: 195-204.

Berillon, G. 2003. Assessing the longitudinal structure of the early hominid foot: A two-dimensional architecture analysis. *Human Evolution* 18: 113-122.

Bock, W. J. and von Wahlert, G. 1965. Adaptation and the form-function complex. *Evolution* 19: 269-299.

Burger, R. 1986. Constraints for the evolution of functionally coupled characters: A nonlinear analysis of a phenotypic model. *Evolution* 40: 182-193.

Cheverud, J. M. 1982. Phenotypic, genetic, and environmental morphological integration in the cranium. *Evolution* 36: 499-516.

Cheverud, J. M., Gunter, P. W., and Dow, M. M. 1989. Methods for the comparative analysis of variation patterns. *Systematic Zoology* 38: 201-213.

Cheverud, J. M., Kohn, L. A. P., Konigsberg, L. W., Leigh S. R. 1992. Effects of fronto-occipital artificial cranial vault modification on the cranial base and face. *American Journal of Physical Anthropology* 88: 323-345.

Conroy, G. C., and Rose, M. D. 1983. The evolution of the primate foot from the earliest primates to the Miocene hominoids. *Foot and Ankle* 3: 342-364.

Czerniecki, J. M. 1988. Foot and ankle biomechanics in walking and running: A review. *The American Journal of Physical Medicine & Rehabilitation* 67: 246-252.

D'Aout, K. and Aerts, P. 2008. The evolutionary history of the human foot. *Advances in Plantar Pressure Measurements in Clinical and Scientific Research*: 44-68.

Day, M. H., and Wood, B. A. 1968. Affinities of the Olduvai hominid 8 talus. *Man* 3: 440-455.

Day, M. H., and Wood, B. A. 1969. Hominoid tali from East Africa. *Nature* 222: 591-592.

DeSilva, J. M. 2009. Functional morphology of the ankle and the likelihood of climbing in early hominins. *Proceedings of the National Academy of Sciences* 106: 6567-6572.

DeSilva, J. M. 2010. Revisiting the "midtarsal break". *American Journal of Physical Anthropology* 141: 245-258.

DeSilva, J. M. and Gill, S. V. 2013. Brief communication: A midtarsal (midfoot) break in the human foot. *American Journal of Physical Anthropology* 151: 495-499.

DeSilva, J. M., Bonne-Annee, R., Swanson, Z., Gill, C. M., Sobel, M., Uy, J. and Gill, S. V. 2015. Midtarsal break variation in modern humans: Functional causes, skeletal correlates, and paleontological implications. *American Journal of Physical Anthropology* 0: 00-000.

DeSilva, J. M., Holt, K. G., Churchill, S. E., Carlson, K. J., Walker, C. S., Zipfel, B., and Berger, L. R. 2013. The lower limb and mechanics of walking in Australopithecus sediba. *Science* 340: 1232999-1-1232999-5.

Doran, D. M. 1997. Ontogeny of locomotion in mountain gorillas and chimpanzees. *Journal of Human Evolution* 32: 323-344.

Dunn, R. H., Tocheri, M. W., Orr, C. M., and Jungers, W. L. 2014. Ecological divergence and talar morphology in gorillas. *American Journal of Physical Anthropology* 153: 526-541.

Elftman, H. and Manter, J. 1935a. Chimpanzee and human feet in bipedal walking. *American Journal of Physical Anthropology* 20: 69-79.

Elftman, H. and Manter, J. 1935b. The evolution of the human foot, with especial reference to the joints. *Journal of Anatomy* 70: 56-67.

Field, A. 2013. Discovering statistics using IBM SPSS statistics: And sex and drugs and rock 'n' roll. London: SAGE Publications Ltd.

Gebo, D. L. 1992. Plantigrady and foot adaptation in African apes: Implications for hominid origins. *American Journal of Physical Anthropology* 89: 29-58.

Gebo, D. L. and Schwartz, G. T. 2006. Foot bones from Omo: Implications for hominid evolution. *American Journal of Physical Anthropology* 000: 00-000.

Grabowski, M. and Porto, A. 2016. How many more? Sample size determination in studies of morphological integration and evolvability. Methods in Ecology and Evolution 1-12.

Grabowski, M., Polk, J. D., and Roseman, C. C. 2011. Divergent patterns of integration and reduced constraint in the human hip and the origins of bipedalism. *Evolution* 65: 1336-1356.

Haile-Selassie, Y., Saylor, B. Z., Deino, A., Levin, N. E., Alene, M., and Latimer, B. M. 2012. A new hominin foot from Ethiopia shows multiple Pliocene bipedal adaptations. *Nature* 483: 565-570.

Hallgrimsson B., Willmore, K., and Hall, B. K. 2002. Canalization, developmental stability and morphological integration in primate limbs. *American Journal of Physical Anthropology* 35: 131-158.

Hallgrimsson, B., Jamniczky H., Young, N. M., Rolian C., Parsons, T. E., Boughner J. C., and Marcucio, R. S. 2009. Deciphering the palimpsest: Studying the relationship between morphological integration and phenotypic covariation. *Evolutionary Biology* 36: 355-376.

Hansen, T. F. 2003. Is modularity necessary for evolvability? Remarks on the relationship between pleiotropy and evolvability. *BioSystems* 69: 83-94.

Hansen, T. F. and Houle, D. 2008. Measuring and comparing evolvability and constraint in multivariate characters. *Journal of Evolutionary Biology* 21: 1201-1219.

Harcourt-Smith, W. E. H, and Aiello, L. C. 1999. An investigation into the degree of hallux abduction of the OH 8 foot. *American Journal of Physical Anthropology* Supplement 28; 145.

Harcourt-Smith, W. 2002. Form and function in the hominoid tarsal skeleton [Dissertation]: University College London, pp. 260.

Harcourt-Smith, W. E. H. and Aiello, L. C. 2004. Fossils, feet and the evolution of human bipedal locomotion. *Journal of Anatomy* 204: 403-416.

Harcourt-Smith, W. E. H., Tallman, M., Frost, S. R., Wiley, D. F., Rohlf, F. J., and Delson, E. 2008. Analysis of selected hominoid joint surfaces using laser scanning and geometric morphometrics: A preliminary report. *Mammalian Evolutionary Morphology*: 373-383.

Hammer, Øyvind, Harper, David A.T., and Paul D. Ryan, 2001. Past: Paleontological Statistics Software Package for Education and Data Analysis. Palaeontologia Electronica, vol. 4, issue 1, art. 4: 9pp., 178kb. http://palaeo-electronica.org/2001_1/past/issue1_01.htm.

Hereford, J., Hansen, T. F., and Houle, D. 2004. Comparing strengths of directional selection: How strong is strong? *Evolution* 58: 2133-2143.

Hunt, K. D., Cant, J. G. H., Gebo, D. L., Rose, M. D., Walker, S. E. and Youlatos, D. 1996. Standardized descriptions of primate locomotor and postural modes. *Primates* 37: 363-387.

Hunt, K. D. 1994. The evolution of human bipedality: Ecology and functional morphology. *Journal of Human Evolution* 26: 183-202.

IBM Corp. Released 2013. IBM SPSS Statistics for Windows, Version 22.0. Armonk, NY: IBM Corp.

Jungers, W. L., Falsetti, A. B., and Wall, C. E. 1995. Shape, relative size, and size adjustments in morphometrics. *Yearbook of Physical Anthropology* 38: 137-161.

Jungers, W. L., Larson, S. G., Harcourt-Smith, W., Morwood, M. J., Sutikna, T., Awe, R. D., and Djubiantono, T. 2009. Descriptions of the lower limb skeleton of *Homo floresiensis*. *Journal of Human Evolution* 57: 538-554.

Jungers, W. L., Harcourt-Smith, W. E. H., Wunderlich, R. E., Tocheri, M. W., Larson, S. G., Sutikna, T., Due, R. A., Morwood, M. J. 2009. The foot of *Homo floresiensis*. Nature 459: 81-84.

Kanamoto, S., Ogihara, N., and Nakatsukasa, M. 2011. Three-dimensional orientations of talar articular surfaces in humans and great apes. *Primates* 52: 61-68.

Ker, R. F., Bennett, M. B., Bibby, S. R., Kester, R. C., and Alexander, R. McN. 1987. The spring arch of the human foot. *Nature* 325: 147-149.

Kidd, R. 1998. The past is the key to the present: thoughts on the origins of human foot structure, function and dysfunction as seen from the fossil record. *The Foot* 8: 75-84.

Kidd, R. S. and Oxnard, C. E. 2002. Patterns of morphological discrimination in selected human tarsal elements. *American Journal of Physical Anthropology* 117: 169-181.

Knigge, R. P., Tocheri, M. W., Orr, C. M., and McNulty, K. P. 2015. Three-dimensional geometric morphometric analysis of talar morphology in extant gorilla taxa from highland and lowland habitats. *The Anatomical Record* 298: 277-290.

Kohler, M. and Moya-Sola, S. 1997. Ape-like or hominid-like? The positional behavior of *Orepithecus bambolii* revisited. *Proceedings of the National Academy of Sciences* 94: 11747-11750.

Kohn, L. A. P., Leigh, S. R., Jacobs, S. C., and Cheverud, J. M. 1993. Effects of annular cranial vault modification on the cranial base and face. *American Journal of Physical Anthropology* 90: 147-168.

Lamy, P. 1986. The settlement of the longitudinal plantar arch of some African Plio-Pleistocene hominids: A morphological study. *Journal of Human Evolution* 15: 31-46.

Lande, R. 1980. The genetic covariance between characters maintained by pleiotropic mutations. *Genetics* 94: 203-215.

Lande, R. and Arnold, S. J. 1983. The measurement of selection on correlated characters. *Evolution* 37: 1210-1226.

Latimer, B. 1991. Locomotor adaptations in Australopithecus afarensis: The issue of arboreality. *Origine(s) de la Bipedie chez les Hominides* 169-176.

Latimer, B. and Lovejoy, C. O. 1989. The calcaneus of *Australopithecus afarensis* and its implications for the evolution of bipedality. *American Journal of Physical Anthropology* 78: 369-386.

Latimer, B. and Lovejoy, C. O. 1990. Hallucal tarsometatarsal joint in *Australopithecus afarensis*. *American Journal of Physical Anthropology* 82: 125-133.

Latimer, B. and Lovejoy, C. O. 1990b. Metatarsophalangeal joints of *Australopithecus afarensis*. *American Journal of Physical Anthropology* 83: 13-23.

Latimer, B., Ohman, J. C., and Lovejoy, C. O. 1987. Talocrural joint in African hominoids: Implications for *Australopithecus afarensis*. *American Journal of Physical Anthropology* 74: 155-175.

Lawler, R. R. 2008. Morphological integration and natural selection in the postcranium of Wild Verrreaux's Sifaka (*Propithecus verreaux verreauxi*). *American Journal of Physical Anthropology* 136: 204-213.

Lewis, O. J. 1972. The evolution of the hallucial tarsometatarsal joint in Anthropoidea. *American Journal of Physical Anthropology* 37: 13-34.

Lewis, O. J. 1980. The joints of the evolving foot. Part III. The fossil evidence. *Journal of Anatomy* 131: 275-298.

Lewton, K. L. 2012. Evolvability of the primate pelvic girdle. *Evolutionary Biology* 39: 126-139.

Lieberman, D. E., Pearson, O. M., and Mowbray, K. M. 2000. Basicranial influence on overall cranial shape. *Journal of Human Evolution* 38: 291-315.

Lieberman, D. E., Ross, C. F., and Ravosa, M. J. 2000. The primate cranial base: Ontogeny, function, and integration. *Yearbook of Physical Anthropology* 43: 117-169.

Lisowski, F. P., Albrecht, G. H., and Oxnard, C. E. 1974. The form of the talus in some higher primates: A multivariate study. *American Journal of Physical Anthropology* 41: 191-215.

Marroig, G. and Cheverud, J. M. 2009. A comparison of phenotypic variation and covariation patterns and the role of phylogeny, ecology, and ontogeny during cranial evolution of New World Monkeys. *Evolution* 55: 2576-2600.

Marroig, G., Shirai, L. T., Porto, A., deOliveira F. B., and De Conto, V. 2009. The evolution of modularity in the mammalian skull II: Evolutionary consequences. *Evolutionary Biology* 36: 136-148.

Microsoft. 2016. Microsoft Excel for Mac. Microsoft Office 365 Subscription. Version 15.29.

Olson, E. C. and Miller, R. L. 1958. *Morphological Integration*. University of Chicago Press: Chicago. 317pp.

Oxnard, C. E., and Lisowski, F. P. 1980. Functional articulation of some hominoid foot bones: Implications for the Olduvai (Hominid 8) foot. *American Journal of Physical Anthropology* 52: 107-117.

Parr, W. C. H., Soligo, C., Smaers, J., Chatterjee, H. J., Ruto, A., Cornish, L., and Wroe, S. 2014. Three-dimensional shape variation of talar surface morphology in hominoid primates. *Journal of Anatomy* 225: 42-59.

Prang, T. C. 2014. Calcaneal robusticity in Plio-Pleistocene hominins: Implications for locomotor diversity and phylogeny. *Journal of Human Evolution* xxx: 1-12.

Prang, T. C. 2015. Rearfoot posture of *Australopithecus sediba* and the evolution of the hominin longitudinal arch. *Nature* 5:17677: 1-9.

Prang, T. C. 2016. The subtalar joint complex of *Australopithecus sediba*. *Journal of Human Evolution* 90: 105-119.

Porto, A., de Oliveira F. B., Shirai, L. T., De Conto, V., and Marroig. 2009. The evolution of modularity in the mammalian skull I: Morphological patterns and magnitudes. *Evolutionary Biology*: 36: 118-135.

Raichlen, D. A., Gordon, A. D., Harcourt-Smith, W. E. H., Foster, A. D., and Haas, Jr., W. R. 2010. Laetoli footprints preserve earliest direct evidence of human-like bipedal biomechanics. *PLoSONE* 5: e9769.

Reeser, L. A., Susman, R. L., and Stern, Jr., J. T. 1983. Electromyographic studies of the human foot: Experimental approaches to hominid evolution. *Foot and Ankle* 3: 391-407.

Rolian, C. 2009. Integration and evolvability in primate hands and feet. *Evolutionary Biology*.

Sarmiento, E. E. 1998. Generalized quadrupeds, committed bipeds, and the shift to open habitats: An evolutionary model of hominid divergence. *American Museum Novitates* 3250: 1-77.

Sarmiento, E. E. and Marcus, L. F. 2000. The os navicular of humans, great apes, OH 8, Hadar and *Oreopithecus*: Function, phylogeny, and multivariate analyses. *American Museum Novitates* 3288:1-38.

Schmitt, D. 2003. Insights into the evolution of human bipedalism from experimental studies of humans and other primates. *The Journal of Experimental Biology* 206: 1437-1448.

Schultz, A. H. 1963. The relative lengths of the foot skeleton and its main parts in primates. *Symposia of Zoological Society of London* 10: 199-206.

Seiffert, E. R. and Simons, E. L. 2001. Astragalar morphology of late Eocene anthropoids from the Fayum Depression (Egypt) and the origins of catarrhine primates. Journal of Human Evolution 41: 577-606.

Susman, R. L. 1983. Evolution of the human foot: Evidence from Plio-Pleistocene hominids. *Foot and Ankle* 3: 365-376.

Szalay, F. S. and Langdon, J. H. The foot of *Oreopithecus*: An evolutionary assessment. *Journal of Human Evolution* 15: 585-621.

Taniguchi, A., Tanaka, Y., Takakura, Y., Kadono, K., Maeda, M., and Yamamoto, H. 2003. Anatomy of the spring ligament. *The Journal of Bone and Joint Surgery* 85: 2174-2178.

Thorpe, S. K. S. and Crompton, R. H. 2005. Locomotor ecology of wild orangutans (*Pongo pygmaeus abelii*) in the Gunung Leuser ecosystem, Sumatra, Indonesia: A multivariate analysis using log-linear modeling. *American Journal of Physical Anthropology* 127: 58-78.

Thorpe, S. K. S. and Crompton, R. H. 2006. Orangutan positional behavior and the nature of arboreal locomotion in Hominoidea. *American Journal of Physical Anthropology* 000: 000-000.

Thorpe, S. K. S., Holder R. L. and Crompton, R. H. 2007. Origin of human bipedalism as an adapatation for locomotion on flexible branches. *Science* 316: 1328-1331.

Tocheri, M. W., Solhan, C. R., Orr, C. M., Femiani, J., Frohlich, B., Groves, C. P., Harcourt-Smith, W. E. H., Richmond, B. G., Shoelson, B., and Jungers, W. L. 2011. Ecological divergence and medial cuneiform morphology in gorillas. *Journal of Human Evolution* 60: 171-184.

Turley, K. and Frost, S. R. 2013. The shape and presentation of the catarrhine talus: A geometric morphometric analysis. *The Anatomical Record* 296: 877-890.

Turley, K. and Frost, S. R. 2014. The ontogeny of talo-crural appositional articular morphology among catarrhine taxa: Adult shape reflects substrate use. *American Journal of Physical Anthropology* 154: 447-458.

Turley, K., Guthrie, E. H., and Frost, S. R. 2011. Geometric morphometric analysis of tibial shape and presentation among catarrhine taxa. *The Anatomical Record* 294: 217-230.

Venkataraman, V. V., Kraft, T. S., DeSilva, J. M., and Dominy, N. J. 2013. Phenotypic plasticity of climbing-related traits in the ankle joint of great apes and rainforest hunter-gatherers. *Human Biology* 85: 309-328.

Warton, D., Durrsma, R., Falster, D., and Taskinen, S. 2013. (Standardised) Major Axis Estimation and Testing Routines. http://web.maths.unsw.edu.au/~dwarton, http://www.bitbucket.org/remkoduursma/smatr

Williams, S. A. 2010. Morphological integration and the evolution of knuckle-walking. *Journal of Human Evolution* 58: 432-440.

Wood, B. 1973. Locomotor affinities of hominoid tali from Kenya. *Nature* 246: 45-46.

Zelditch, M. L. 1987. Evaluating models of developmental integration in the laboratory rat using confirmatory factor analysis. *Systematic Zoology* 36: 368-380.

Zelditch, M. L. 1988. Ontogenetic variation in patterns of phenotypic integration in the laboratory rat. *Evolution* 42: 28-41.

Zipfel, B., DeSilva, J. M.m and Kidd, R. S. 2009. Earliest complete hominin fifth metatarsal – Implications for the evolution of the lateral column of the foot. *American Journal of Physical Anthropology* 140: 532-545.

Zipfel, B., DeSilva, J. M., Kidd, R. S., Carlson, K. J., Churchill, S. E. and Berger, L. R. 2011. The foot and ankle of *Australopithecus sediba*. *Science* 333: 1417-1420.